Complex Aero Engine Intake Aerodynamics

Pavlos K Zachos, David G. MacManus, Daniel Gil

Propulsion Engineering Centre - Cranfield University, United Kingdom

XXIII Biennial Symposium on Measuring Techniques in Turbomachinery, Transonic and Supersonic Flows in Cascades and Turbomachines, Stuttgart, Germany 2016

www.cranfield.ac.uk

Agenda

- Introduction and rationale
- Experimental facility and methods
  - Rig layout
  - Instrumentation setup and data processing
  - Test matrix
- Flow velocity measurements
  - AIP time averaged and unsteady flow analysis
  - Distortion metrics and statistics
- CFD methods
- What about pressure distortion ?
- Wrap up

Centre for Propulsion Engineering – Experimental aerodynamics – Complex aero engine intakes

Cranfield UNIVERSITY

- Future air vehicles – importance of engine system integration.
- Compact configurations – sufficient operability margin.
- Advanced civil configurations - partially embedded engines.

Distributed propulsion

CIVIL

- Complex engine installations and intakes.
- Distorted, unsteady flow fields presented to aero-engine.
- 8x5 pressure rake can't measure that!

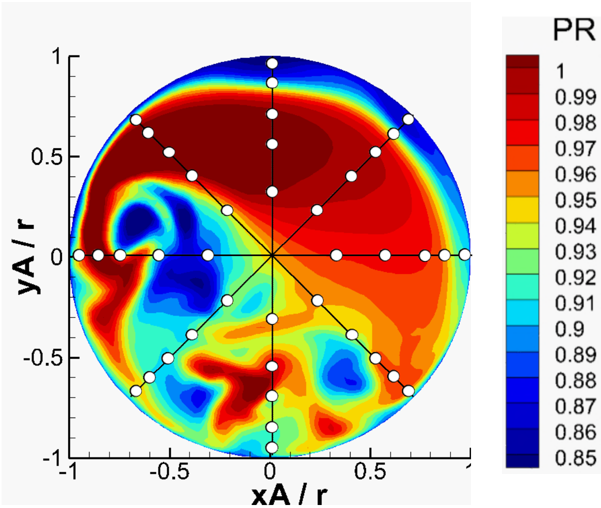

Rationale and current challenges

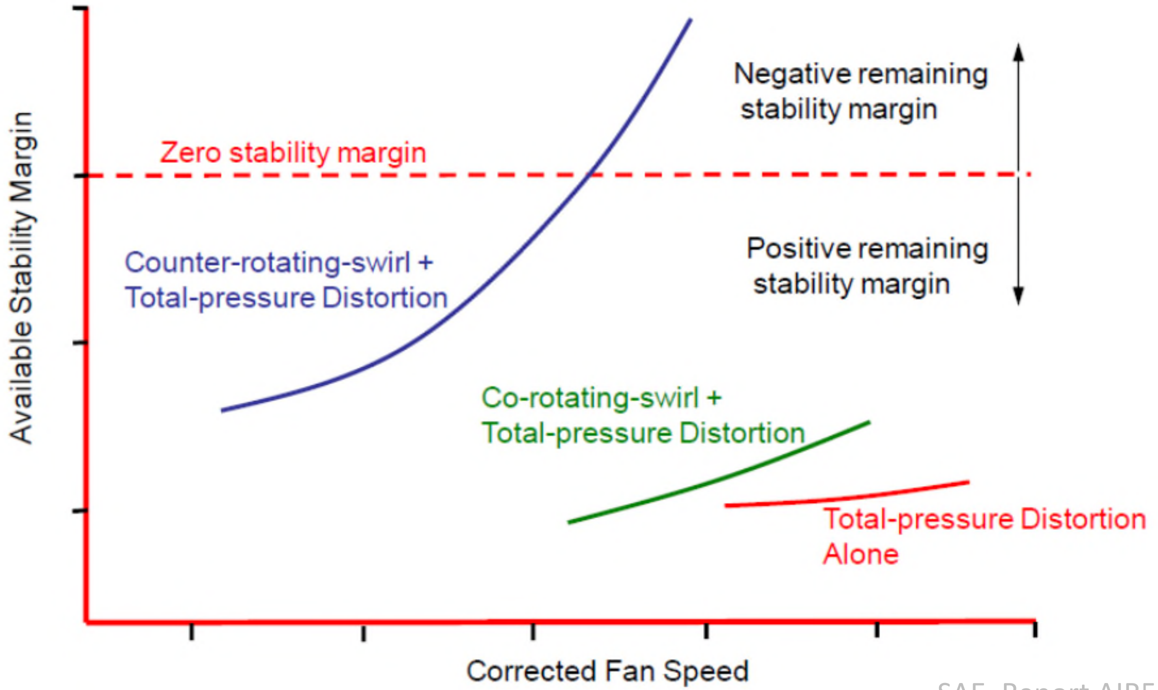

SAE, Report AIR5686

- ❑ Co-rotating swirl + pressure distortion → Surge margin loss.
- ❑ Counter-rotating swirl + pressure distortion → Dramatic surge margin loss.
- ❑ Need for synchronous assessments of pressure and swirl distortion.
- ❑ No swirl data exist to support the understanding of swirl characteristics.

→ **Stall inception?**

→ **PIV ?**

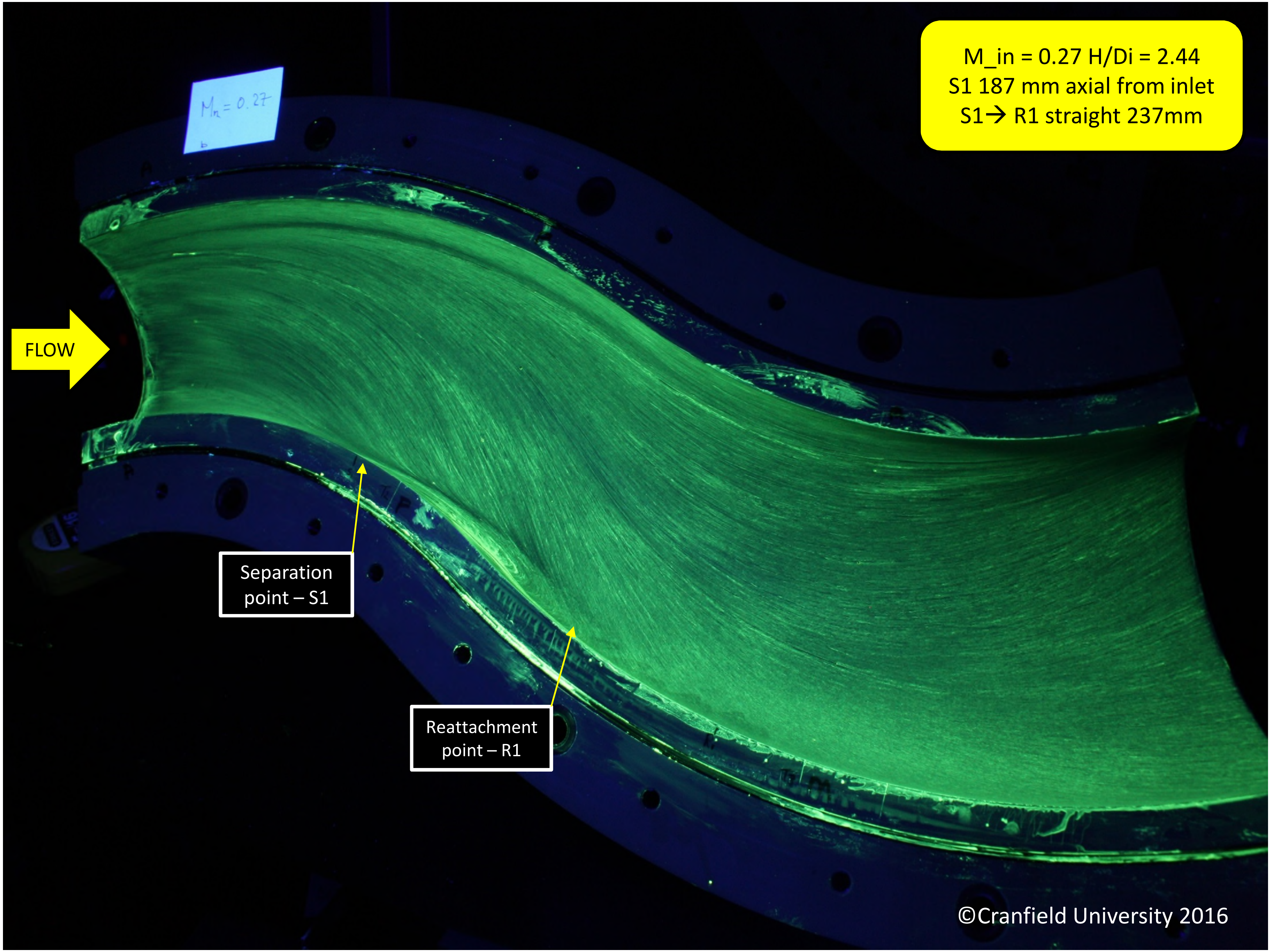
M_in = 0.27 H/Di = 2.44
S1 187 mm axial from inlet
S1→ R1 straight 237mm
FLOW
$M_n = 0.27$
Separation point – S1
Reattachment point – R1
©Cranfield University 2016

Complex intake facility - Rig layout

Cranfield UNIVERSITY

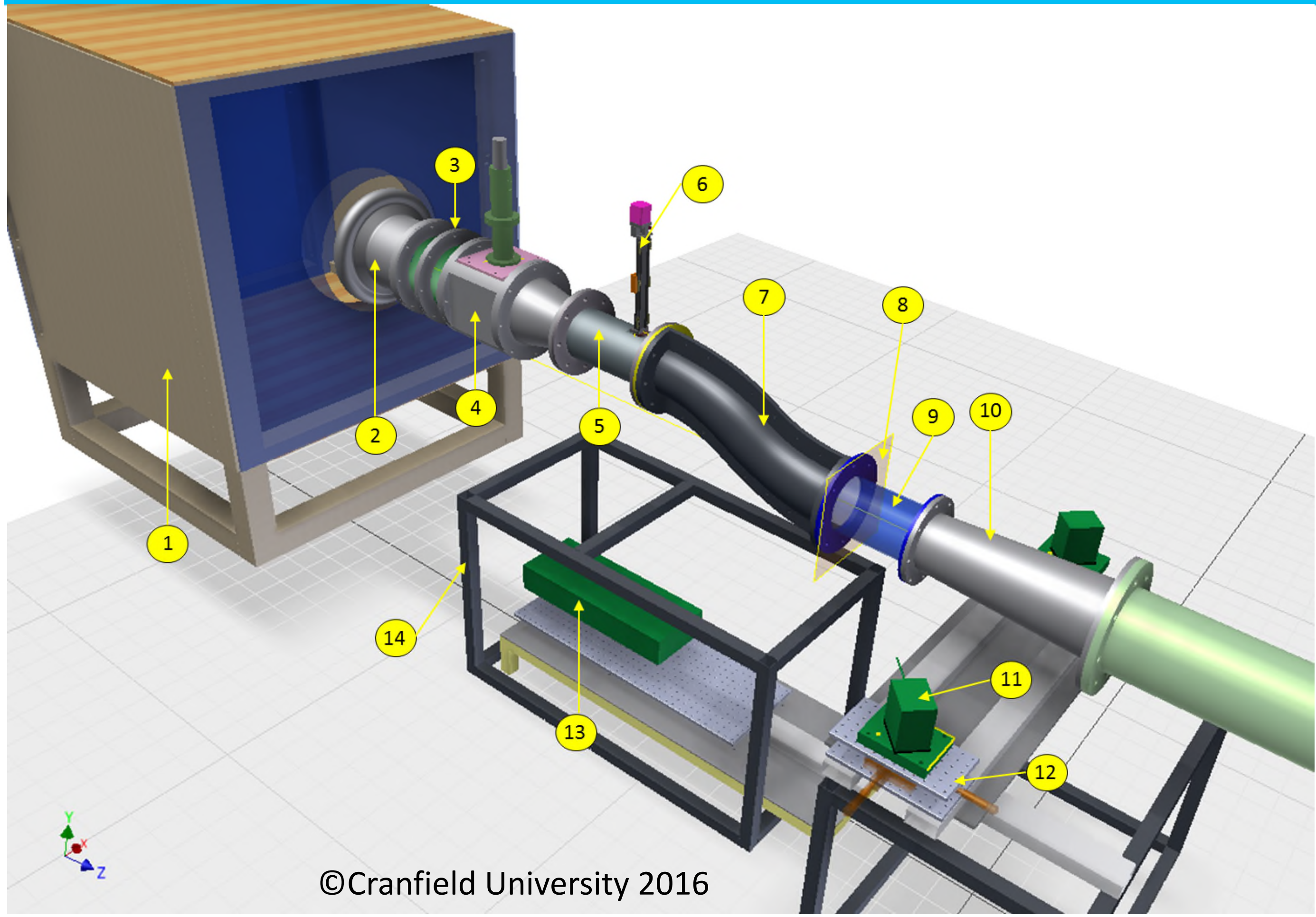

1: Seeding chamber
2: Intake
3: Flow measurement section
4: Vortex generator section
5: Straight section
6: HWA traverse station
7: S-duct
8: Measurement plane
9: Optical working section
10: Suction system
11: PIV camera
12: Camera traverse system
13: Laser
14: Support system

Experimental facility & methods
Rig layout

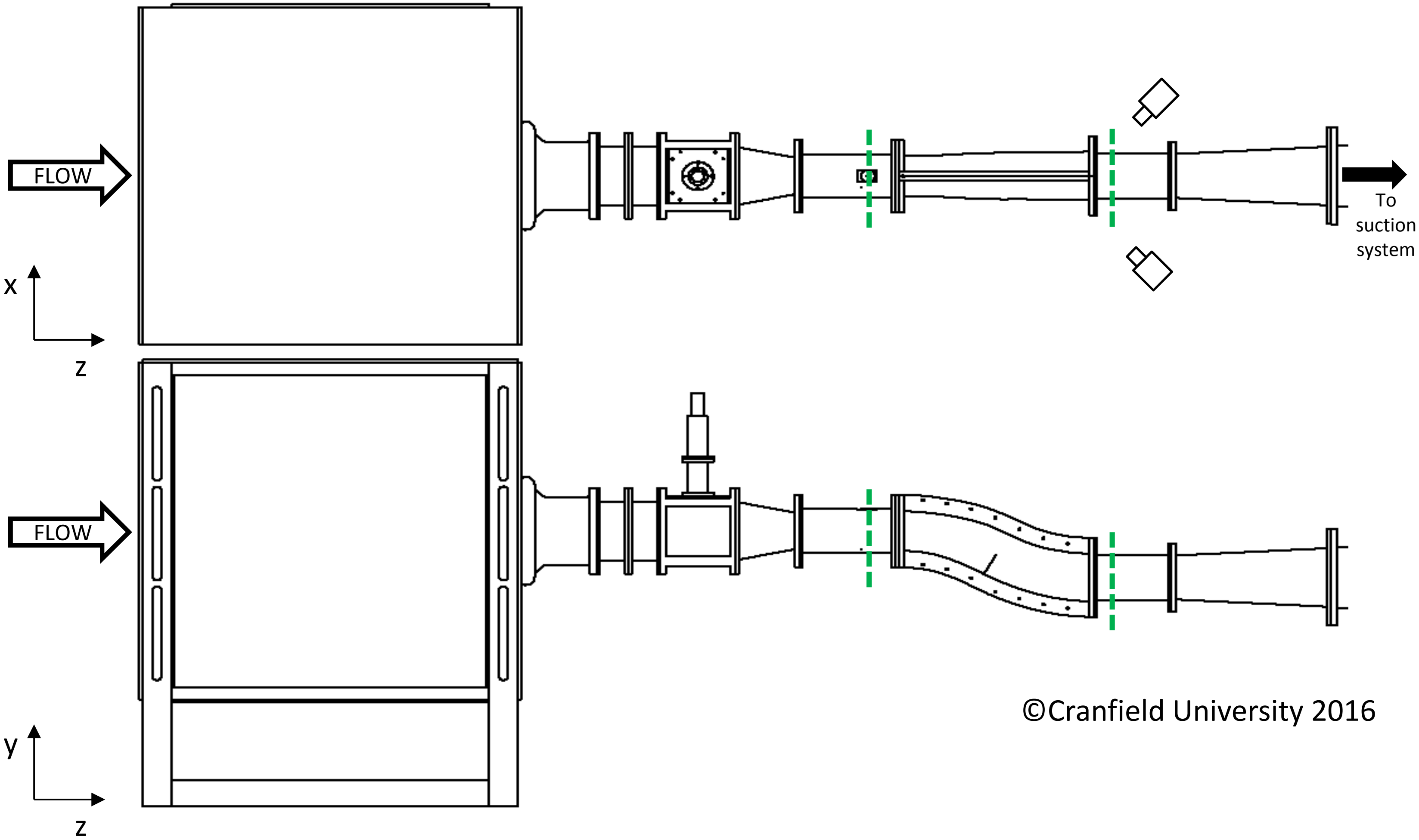

©Cranfield University 2016

Experimental facility & methods
Rig layout

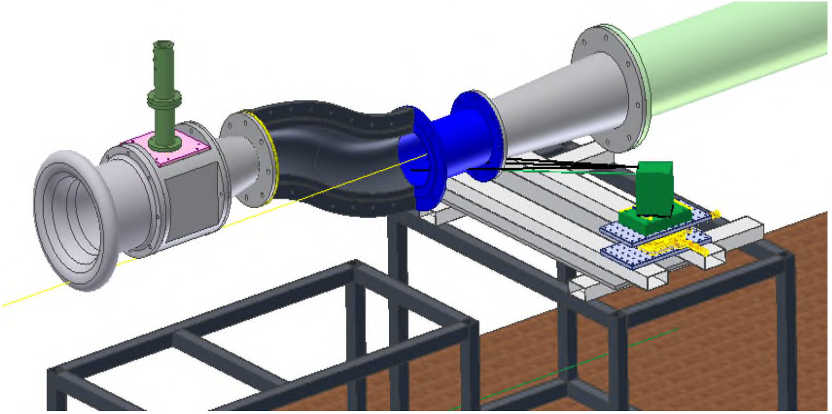

Low offset S-duct
Inlet diameter = 121 mm
Area ratio = 1.52
Offset to Inlet Diameter ratio = 1.34

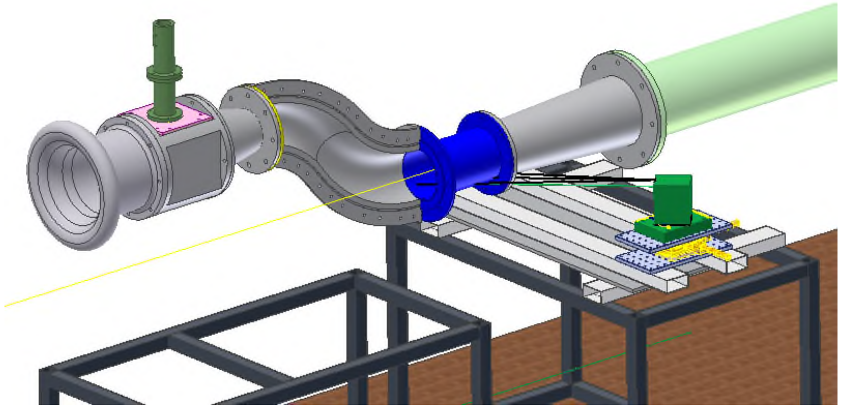

High offset S-duct
Inlet diameter = 121 mm
Area ratio = 1.52
Offset to Inlet Diameter ratio = 2.44

- Suck-down configuration.
- Maximum Mach number at the S-duct inlet ~ 0.8
- Circular working section diameter = 150 mm.
- Glass wall thickness = 5 mm.
- Capability to generate additional, prescribed distortion at the S-duct inlet.

Experimental facility & methods
Instrumentation setup

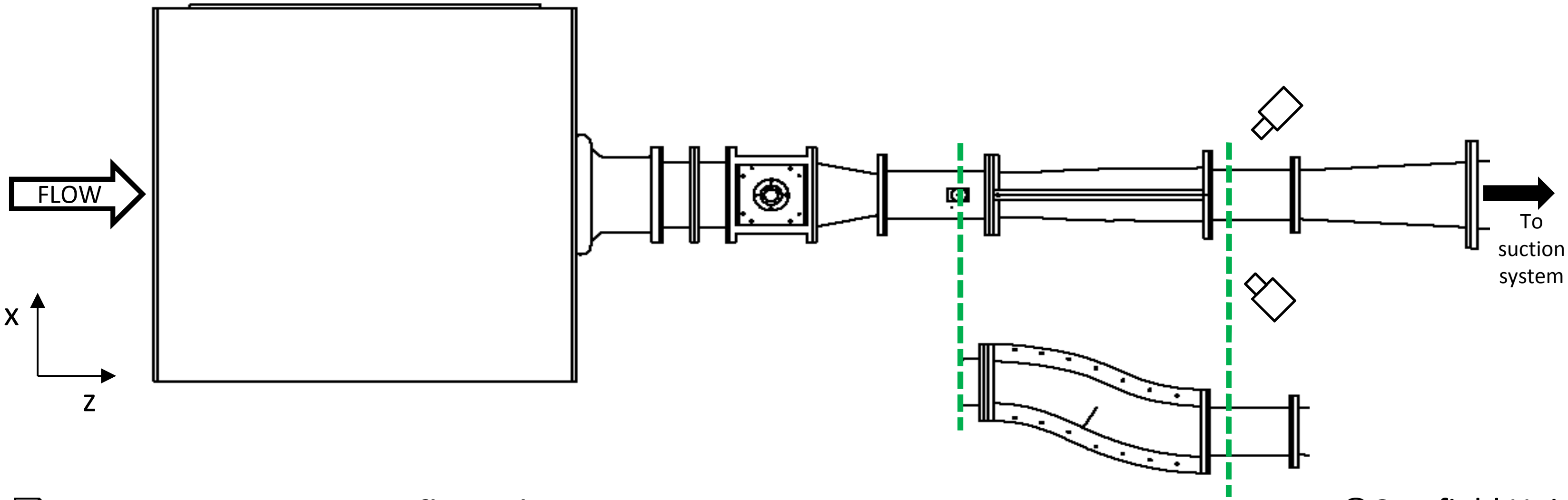

©Cranfield University 2016

- 3C-2D PIV at a cross flow plane.
- S-PIV plane at $0.25D_{out}$ i.e. 37 mm downstream of S-duct exit.
- Dual cavity pulsed Nd:YAG laser – 200 mJ/pulse – acquisition rate 7.5Hz
- 2x TSI PowerView Plus cameras at 4MP (2048 x 2048 px).
- 45^o off-axis arrangement.
- Field of view = 150 mm
- Upstream measurement plane at 0.9Di

Experimental facility & methods
Instrumentation setup

Cranfield UNIVERSITY

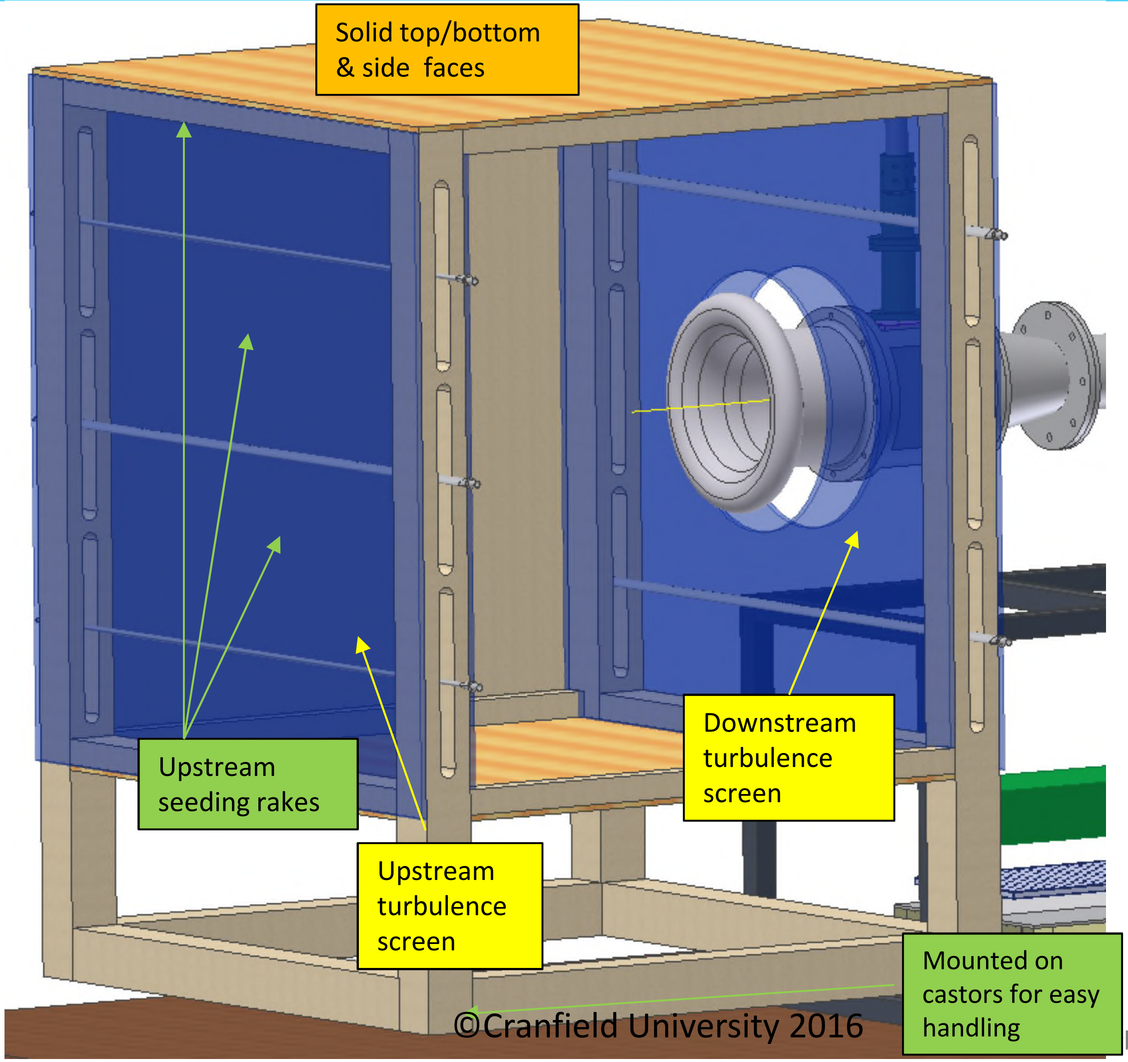

- Seeding chamber to distribute seeding flow: Area ratio = 35:1
- Integrated seeding rakes – upstream and downstream.
- Solid top/bottom/side walls.
- Flow velocity ~2 m/s at chamber face.
- Turbulence generation mesh at front and back face.

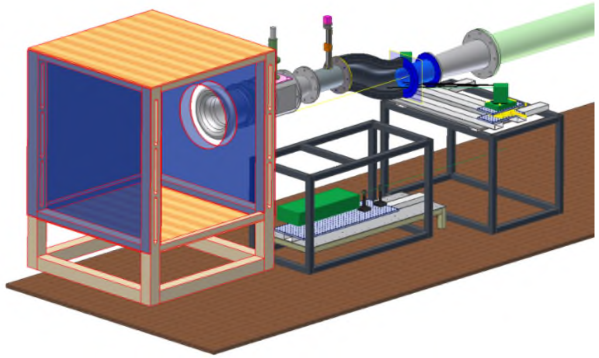

Experimental facility & methods
SPIV workflow

Illumination

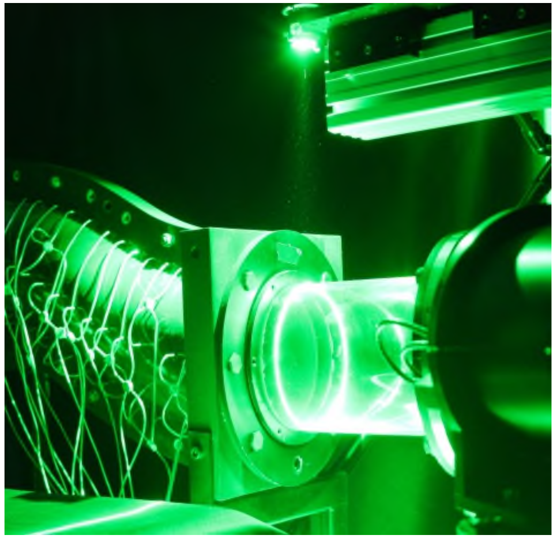

Flow image & filtering

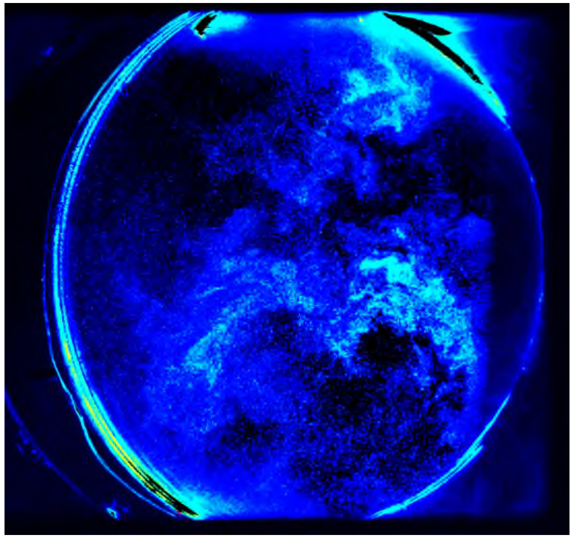

3 component velocity field

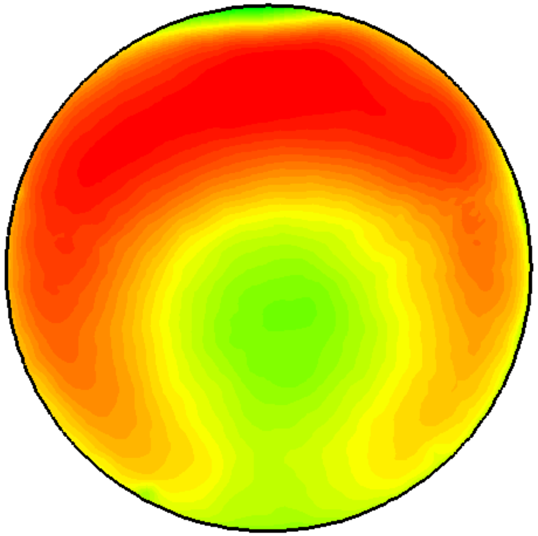

- TSI Insight4G.
- 1,000 images per dataset.
- Image pre-filtering.
- Five plane calibration with 3rd order polynomials.
- Recursive Nyquist processing → 64x64/32x32 with 50% window overlap.
- Final spatial resolution 1.2 x 1.2 mm i.e. 0.8% D_{out} → **9,000 velocity vectors per plane.**

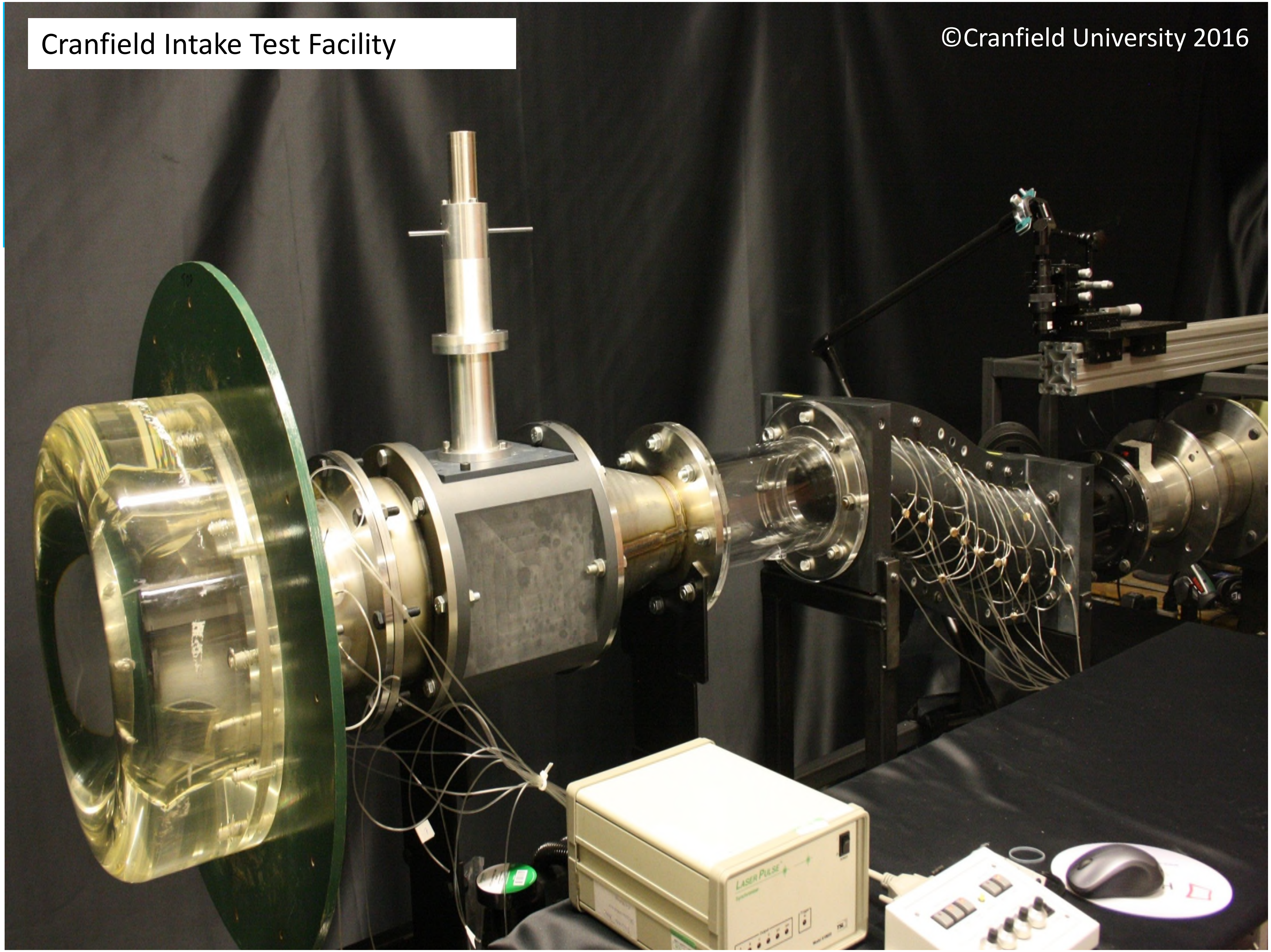
Cranfield Intake Test Facility
©Cranfield University 2016
LASER PULSE

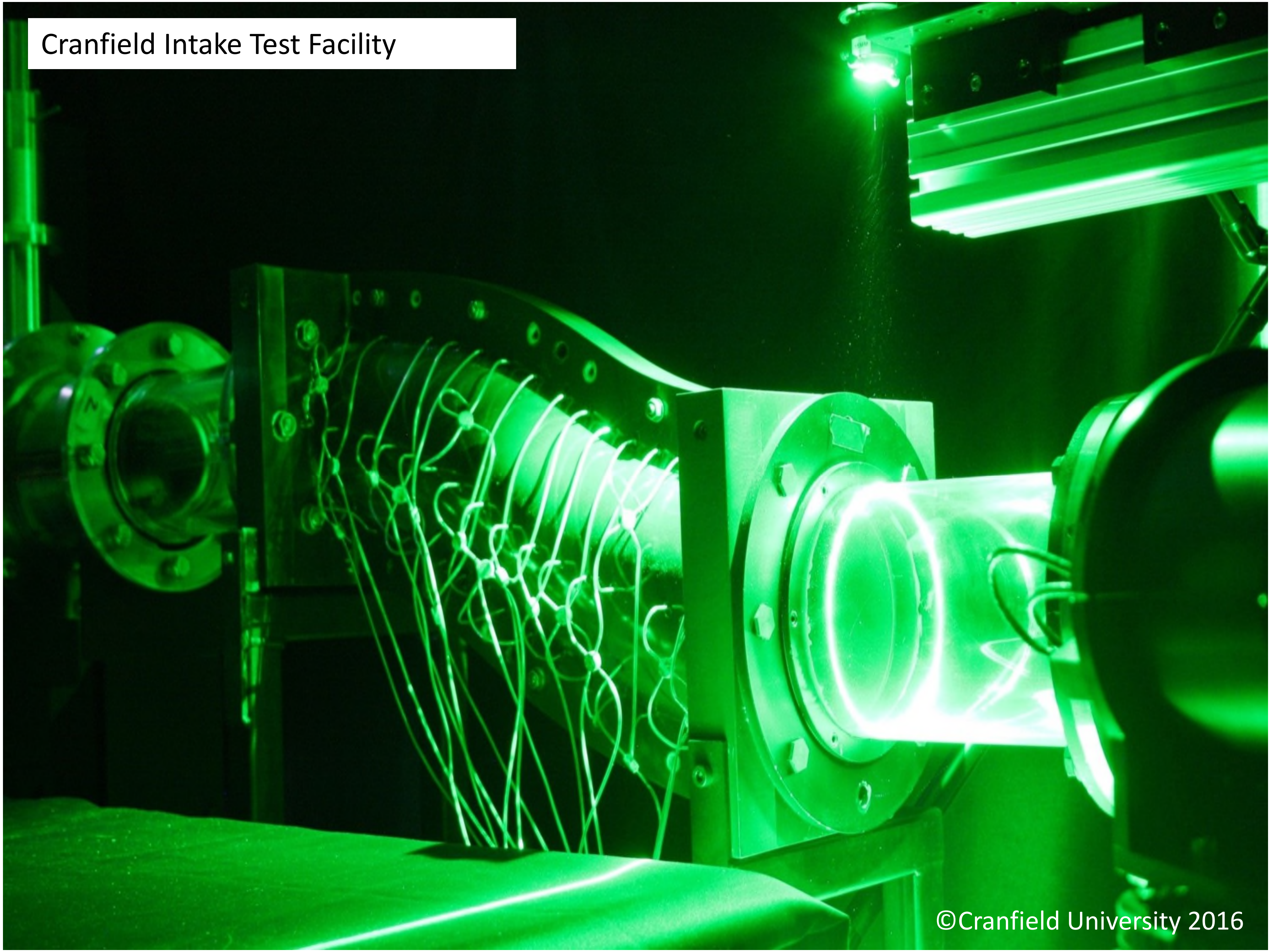
Cranfield Intake Test Facility
©Cranfield University 2016

Experimental facility & methods
Case matrix

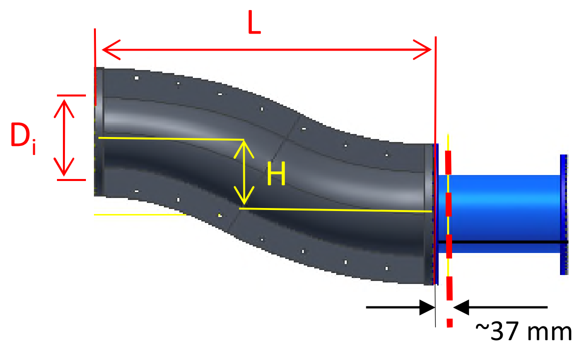

		Inlet Mach	Inlet Re_D
	D_i = 121.6 mm A_{out} / A_{in} = 1.52 H / D_i = 1.34 L / D_i = 5.0	0.27 0.45 0.6	5.9e+5 9.9e+5 13.2e+5
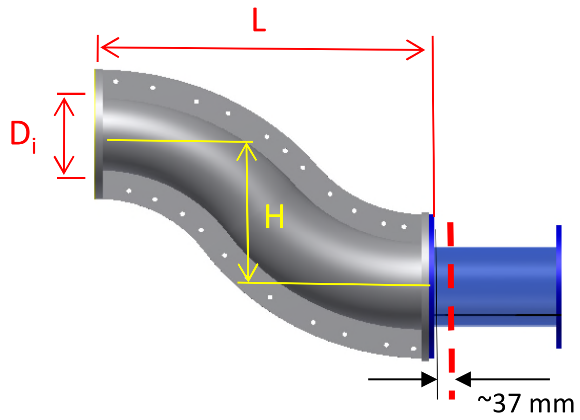	D_i = 121.6 mm A_{out} / A_{in} = 1.52 H / D_i = 2.44 L / D_i = 4.95	0.27 0.45 0.6	6.01e+5 10.05e+5 13.8e+5

AIP flow analysis
Time averaged out of plane velocity

M_{in} = 0.27 $\qquad$ M_{in} = 0.6

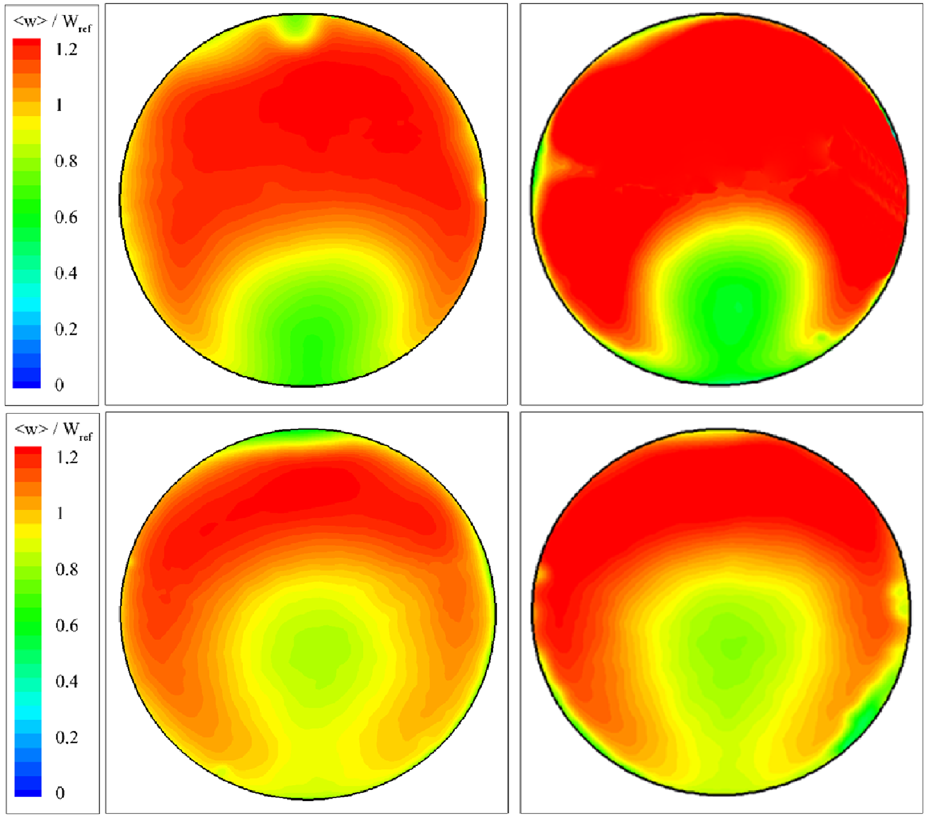

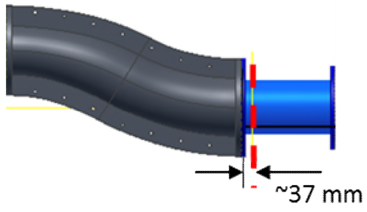

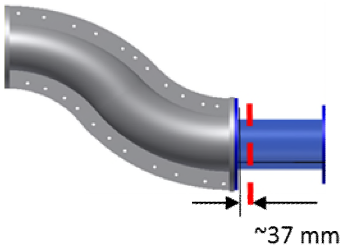

- ❑ Expected low velocity region.
- ❑ More pronounced at HO.
- ❑ Stronger secondary flows.
- ❑ Upstream movement of centreline separation point.
- ❑ Loss migrates to a more central location at the HO S-duct.
- ❑ Affects distortion descriptors.
- ❑ Top separation captured.
- ❑ Weak effect of Mach / Re.

AIP flow analysis
Unsteady out of plane velocity

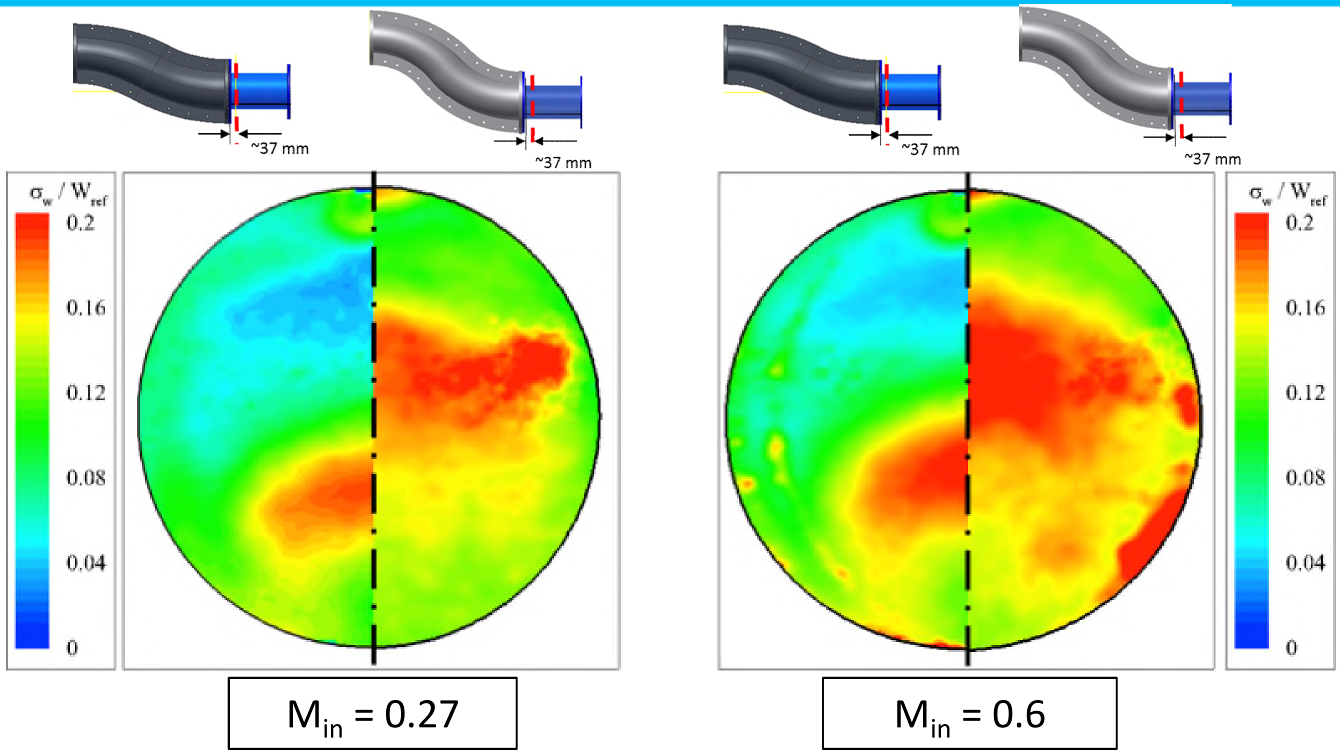

- ❑ At the LO max unsteadiness co-located with max loss.
- ❑ Unsteadiness reduces close to the wall.
- ❑ < 5% across the rest of the AIP - ~10% at the top loss region.
- ❑ Weak effect of Mach.

- ❑ More extensive at HO – higher peak values ~20%.
- ❑ More central position – associated with main loss zone.
- ❑ Spanwise position affects turbomachinery performance.
- ❑ No region of low unsteadiness.

AIP flow analysis
Unsteady radial velocity

Cranfield UNIVERSITY

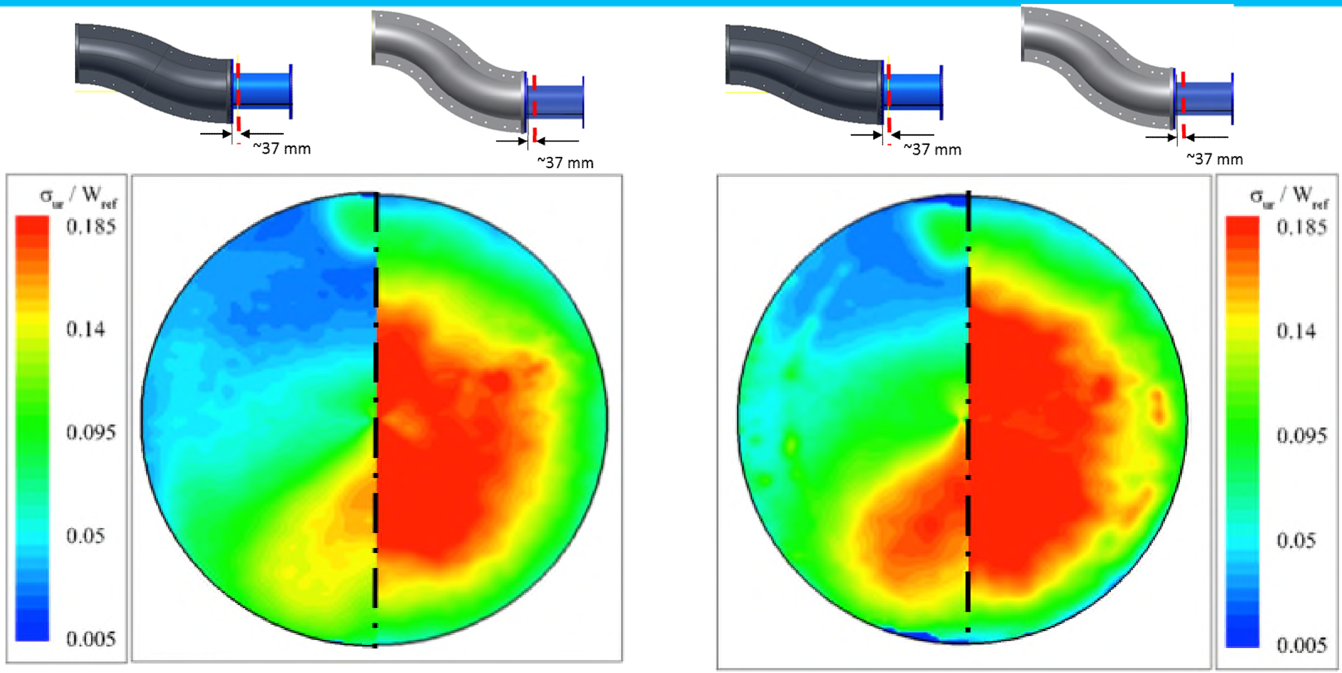

M_{in} = 0.27

M_{in} = 0.6

- At the LO max unsteadiness at the lower AIP part.
- At the HO – higher unsteadiness – closer to the AIP center.
- Mach number doubles the highly unsteady regions in both cases.

AIP flow analysis
Unsteady circumferential velocity

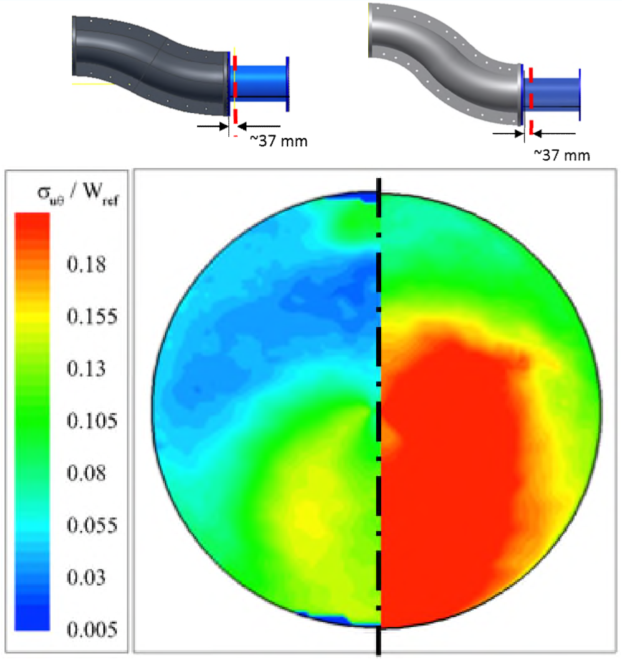

M_{in} = 0.27

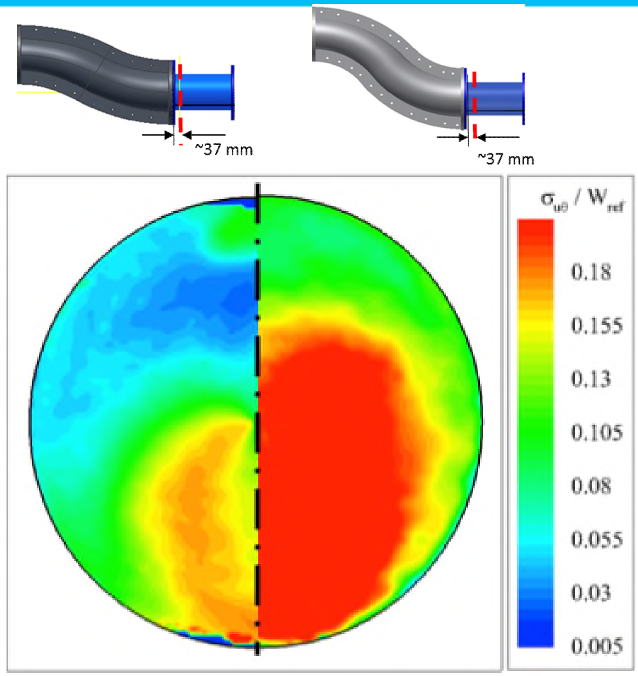

M_{in} = 0.6

- At the LO max unsteadiness close to the max loss region.
- Greater radial position than unsteady out of plane velocity.
- Distinct high and low unsteadiness regions.
- Distribution unaffected by Mach number – levels increase.

- At the HO similar topology – higher levels.
- Contrast with out of plane velocity unsteadiness.
- Modest effect of Mach number.

AIP flow analysis
Time averaged radial Reynolds stress

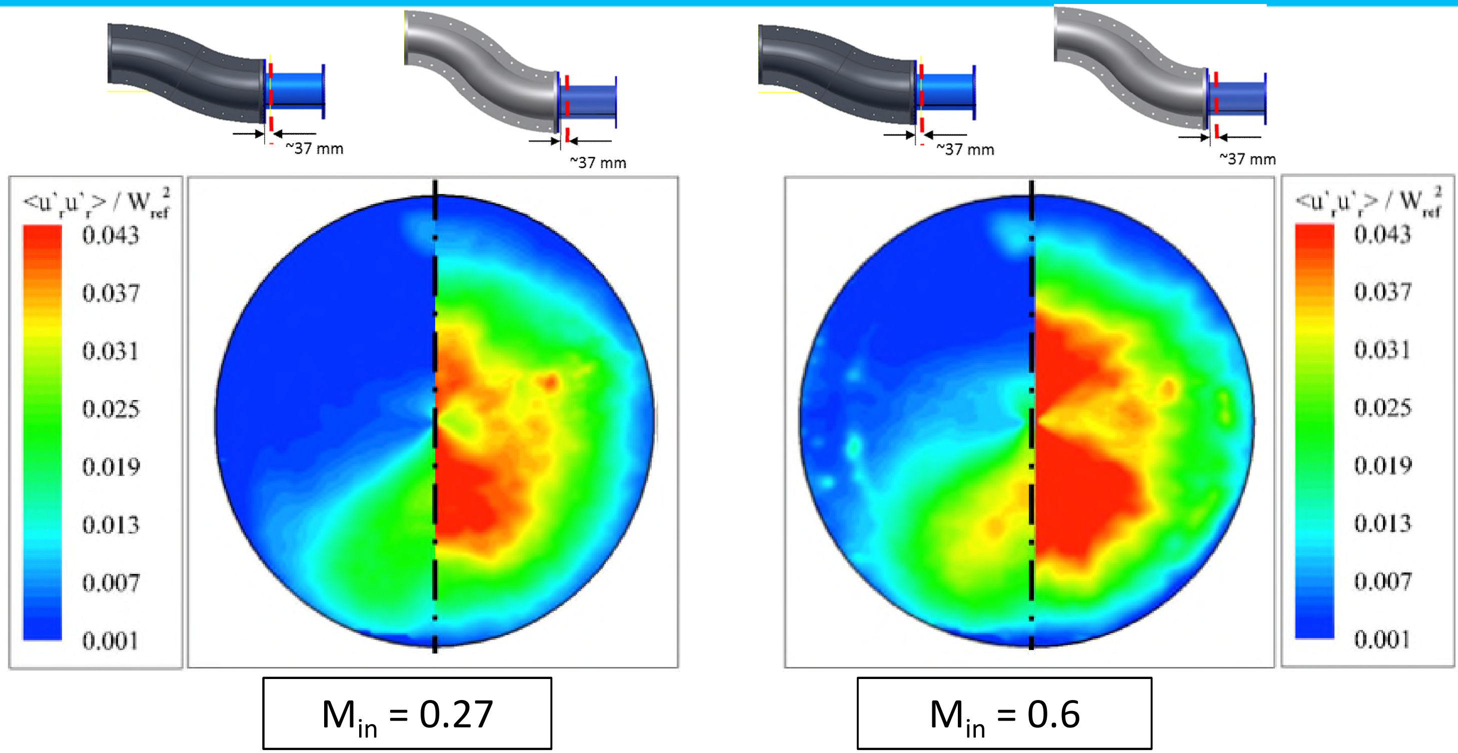

- ❑ HO shows a vertical oscillatory pattern.
- ❑ Extends across top and bottom parts.
- ❑ Associated with the shedding of the separated flow within the duct.

- ❑ Inlet Mach does not affect the topology.
- ❑ Slight increase at the unsteadiness and extent of the unsteady regions.

AIP flow analysis
Time averaged swirl angle

M_{in} = 0.27 M_{in} = 0.6

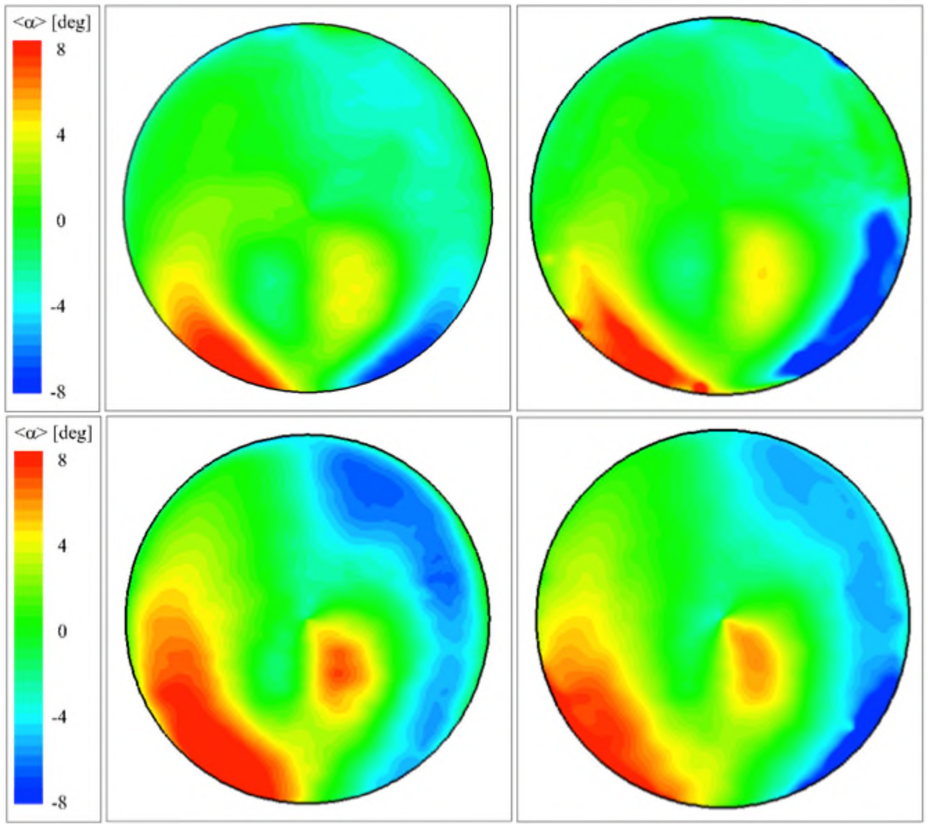

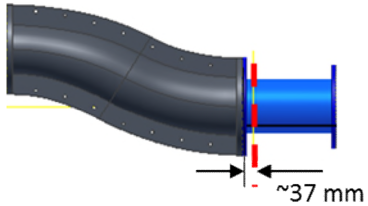

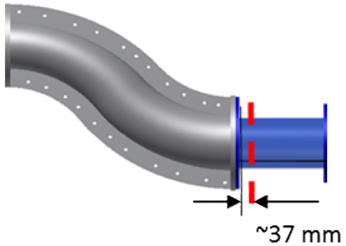

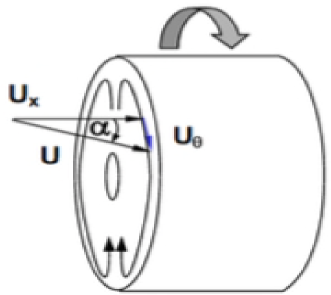

- Localised at the LO.
- Restricted at the bottom part of AIP.
- High swirl angle levels at the HO – covering ~40% of the AIP.
- Similar levels in both cases.

AIP flow analysis
Unsteady swirl angle

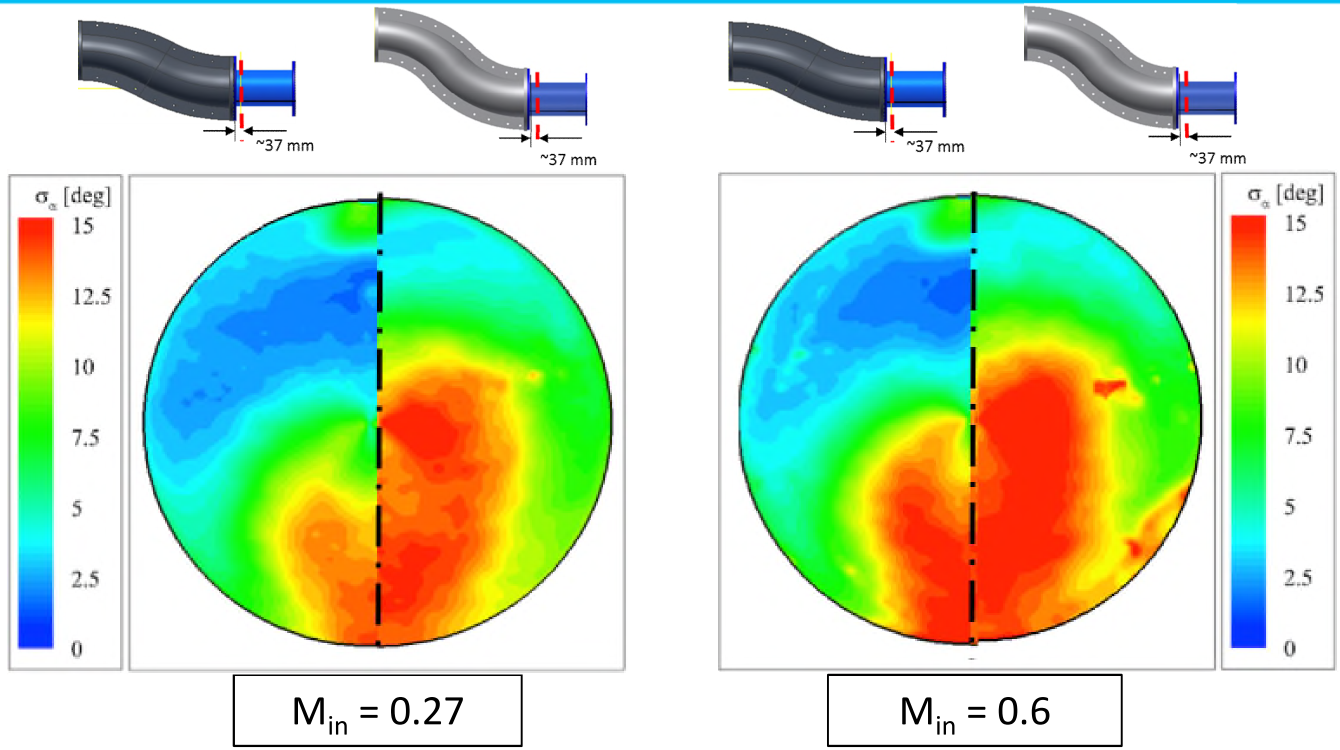

- ❑ Substantial swirl angle variations for both cases.
- ❑ At LO more localised unsteady swirl – mainly dictated by the unsteady circumferential velocity.
- ❑ More extended regions at HO – aligned with highly unsteady regions of w and uθ.
- ❑ Both out of plane and circumferential components contribute equally.

AIP flow analysis
Instantaneous velocity and swirl

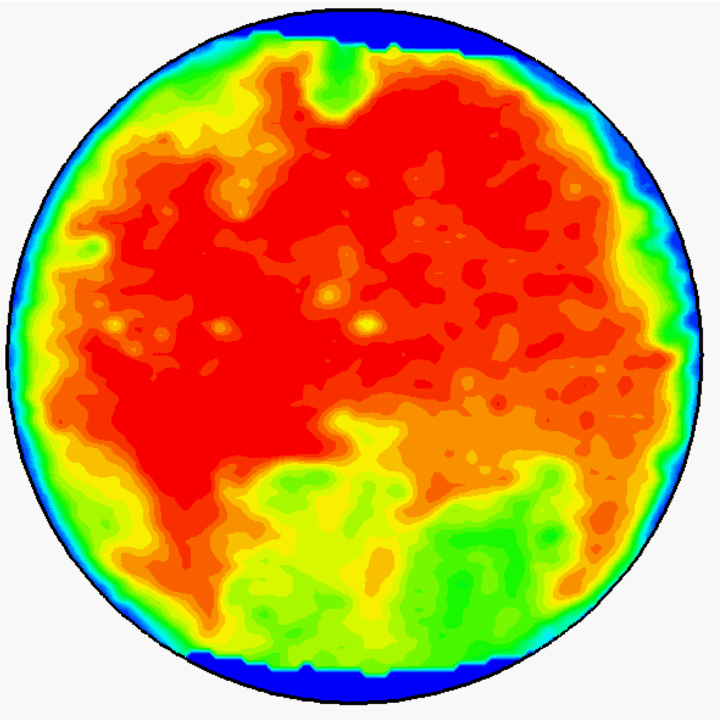

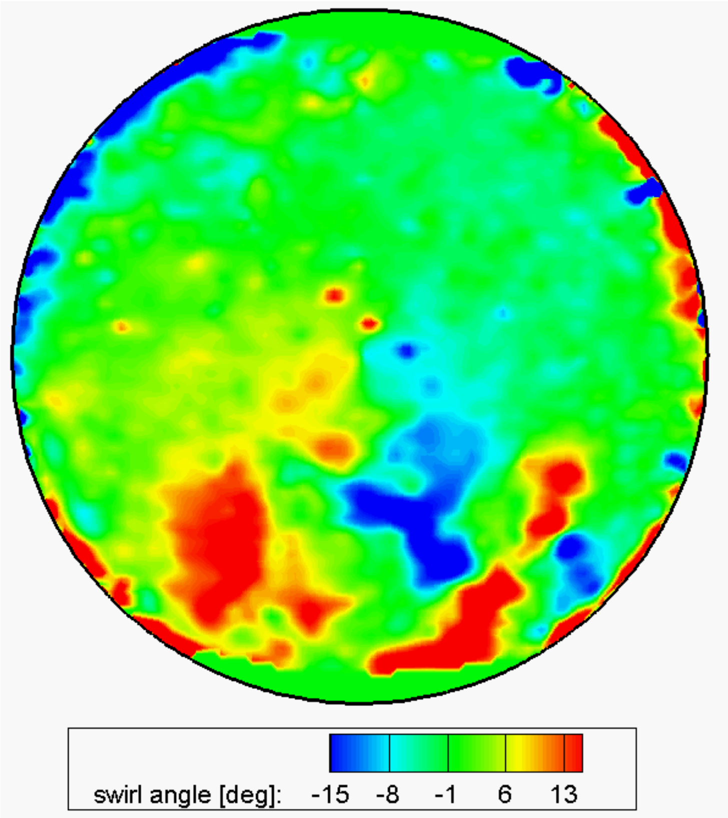

AIP flow analysis
Instantaneous velocity and swirl

Very challenging for an 8x5 rake !!!

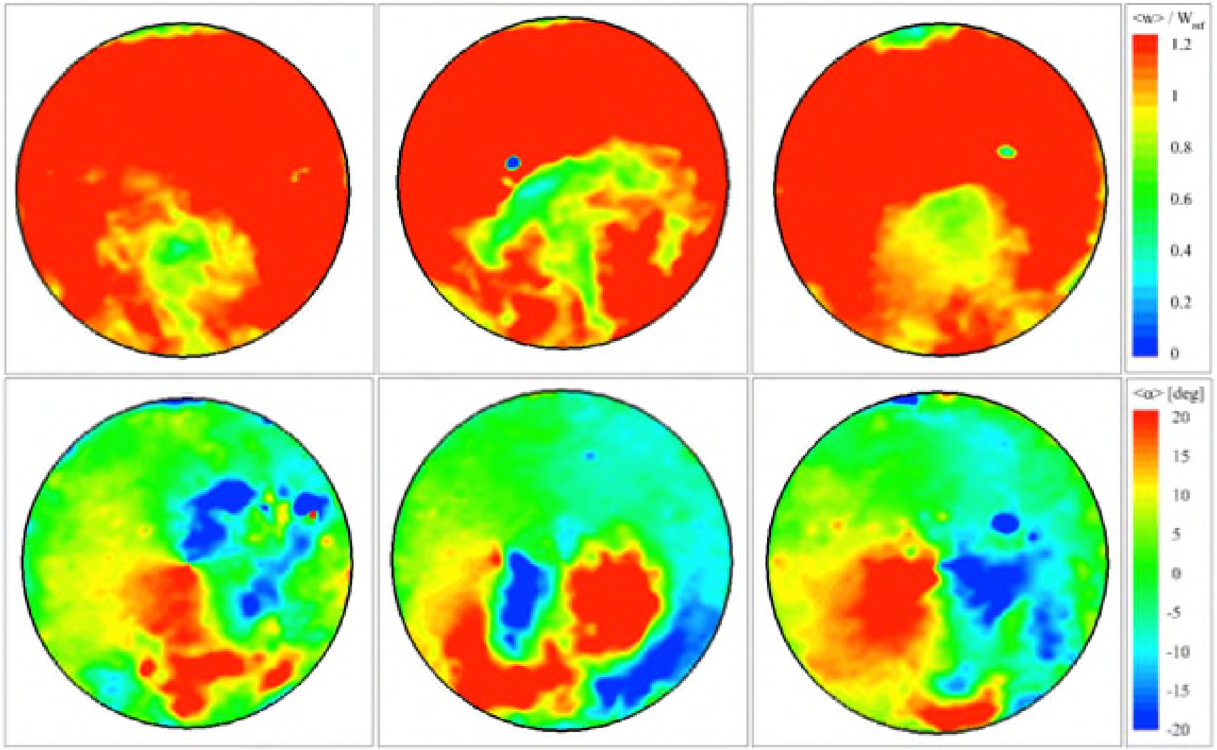

Low offset S-duct, M_{in} = 0.27

AIP flow analysis
Time averaged vorticity

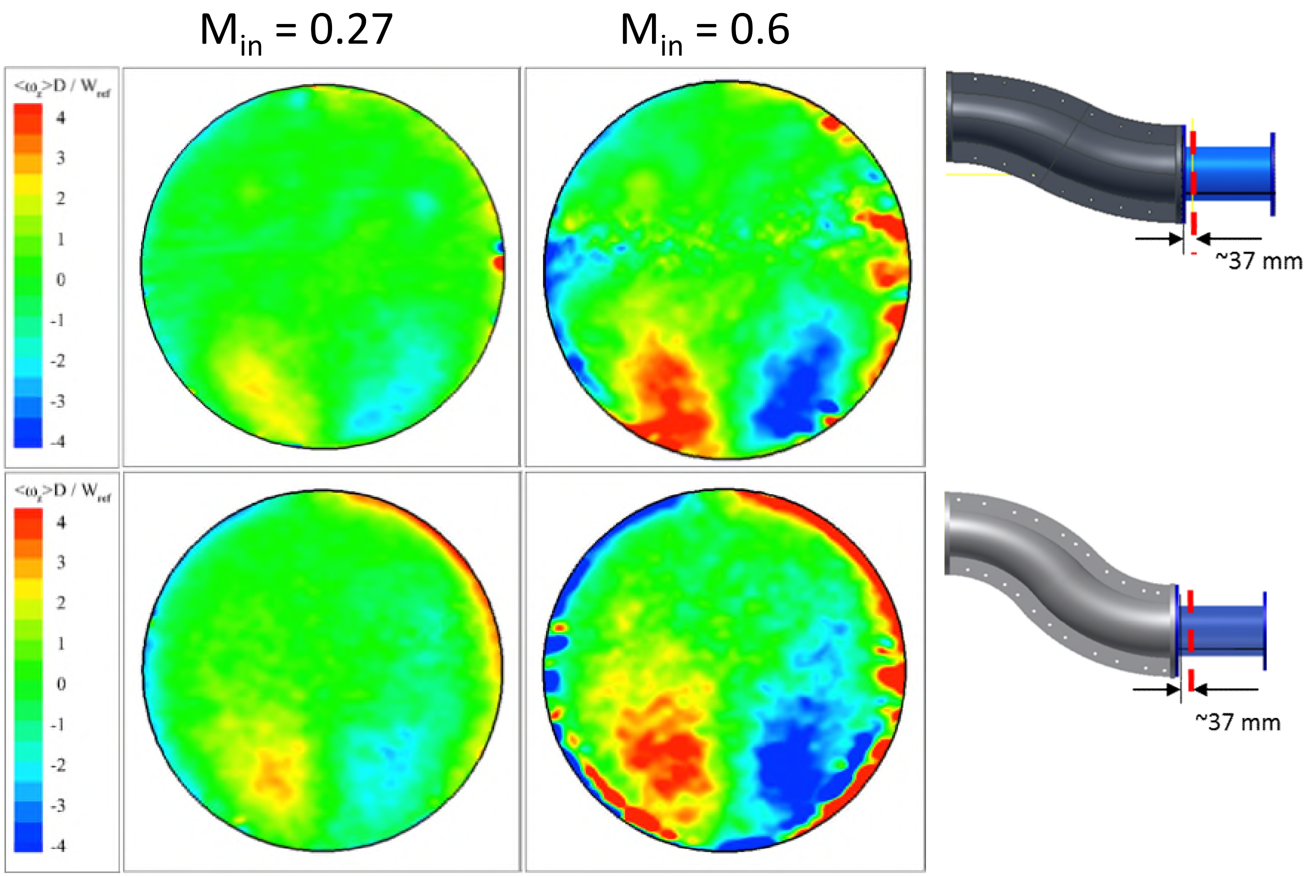

- ❑ Highest levels at bottom part of the AIP.
- ❑ At LO vortex centers are further apart and at a lower position.
- ❑ Peak vorticity does **not** coincide with peak out of plane velocity unsteadiness regions.
- ❑ Not necessarily associated with separation point.

Flow distortion metrics
SAE Swirl intensity

$$SI(i) = \frac{\sum_{k=1}^{m} SS_{i,k}^{+} \cdot \theta_{i,k}^{+} + \sum_{k}^{m} \left| SS_{i,k}^{-} \right| \cdot \theta_{i,k}^{-}}{360}$$

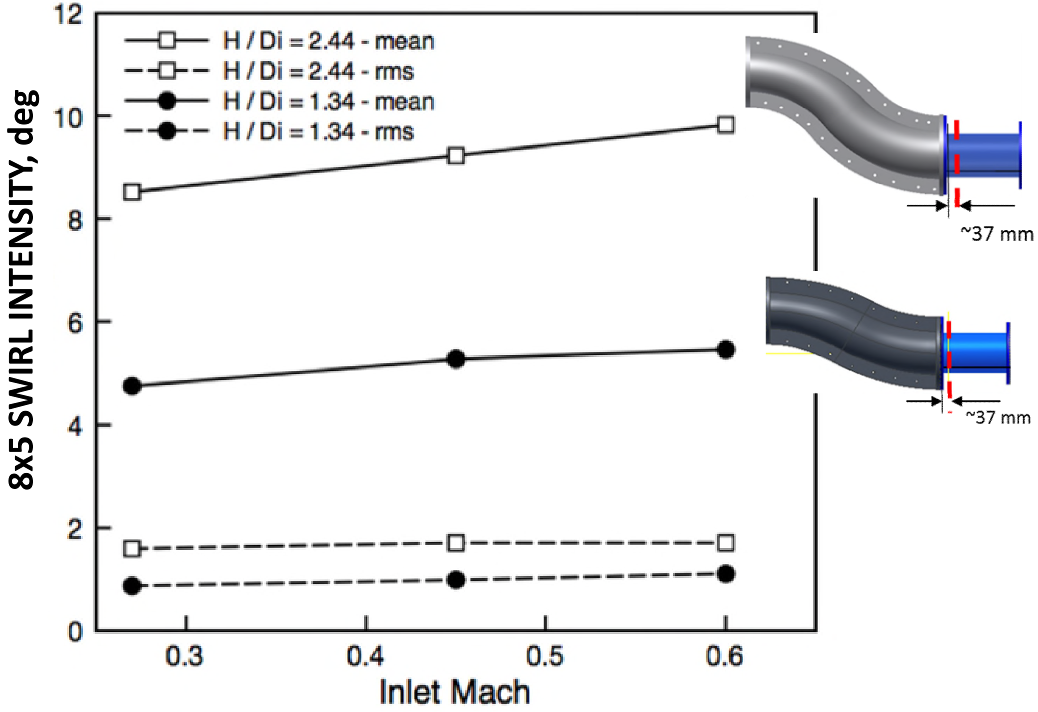

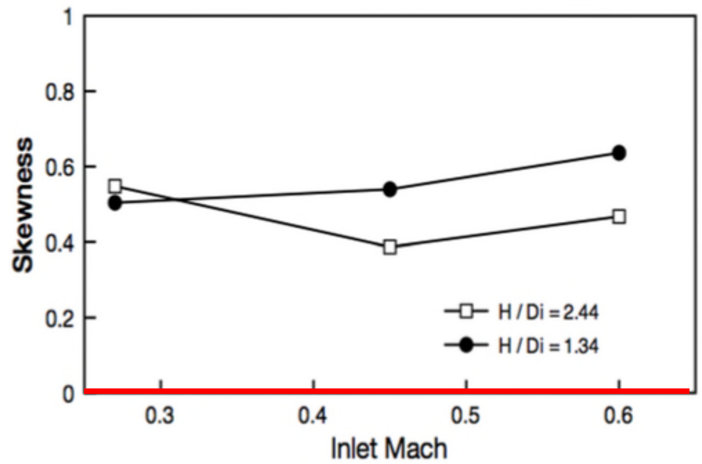

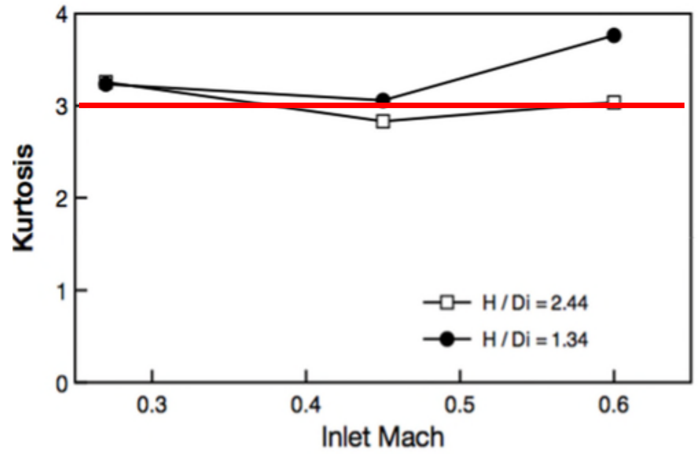

Flow distortion metrics SC60

$$SC(60) = \frac{\mathrm{Max}(u_\theta[60])}{W_{ref}}$$

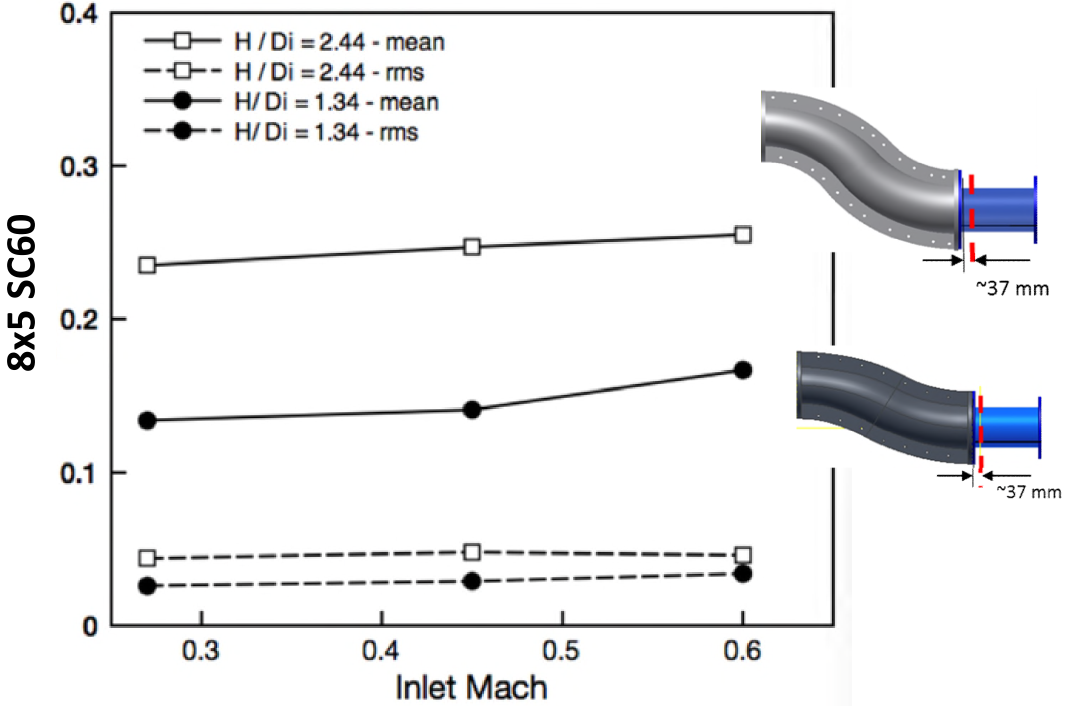

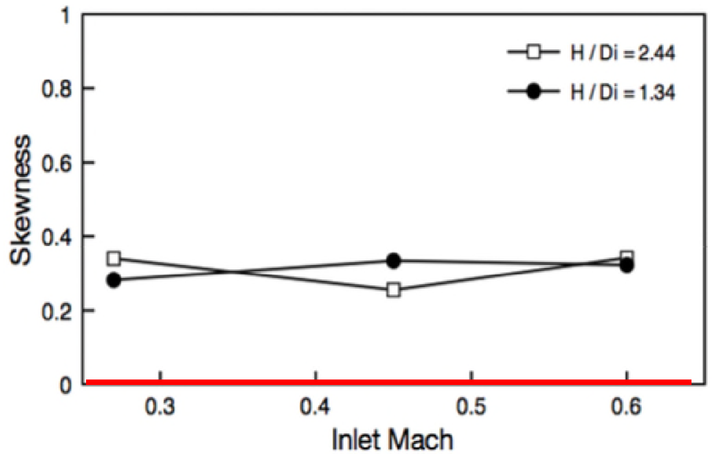

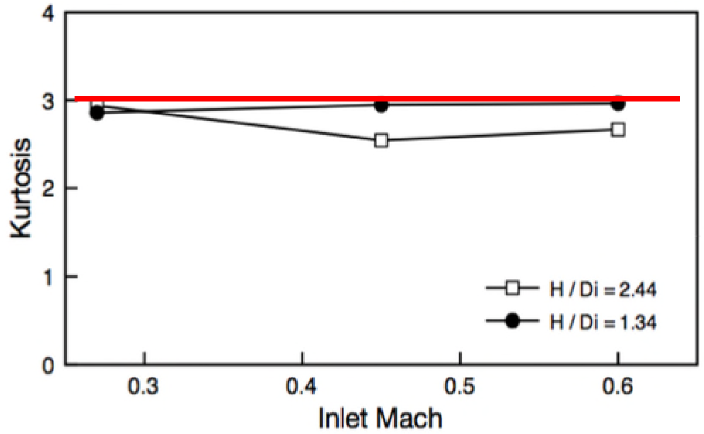

Flow distortion metrics
SI - SC60 maps

PIV velocity field

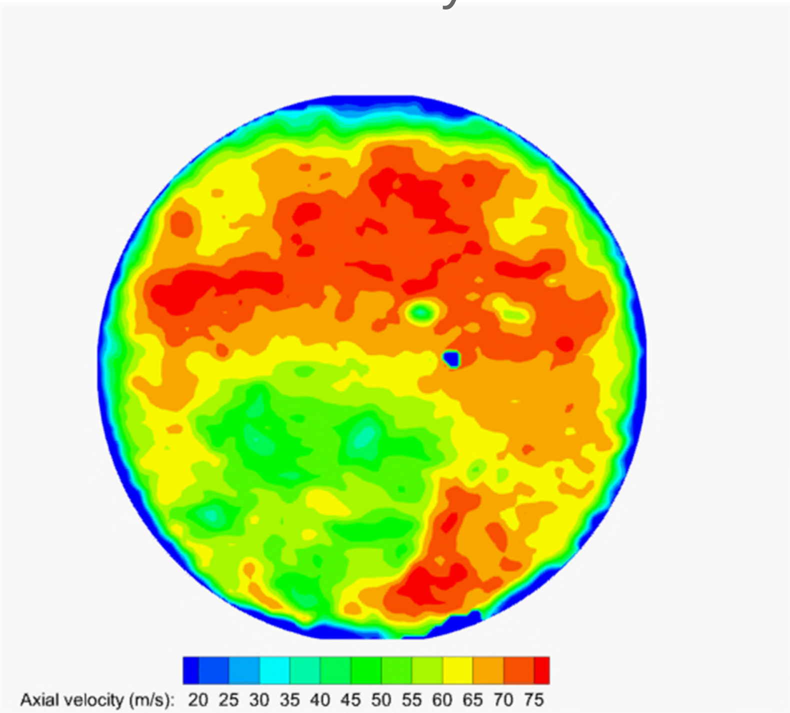

Swirl intensity

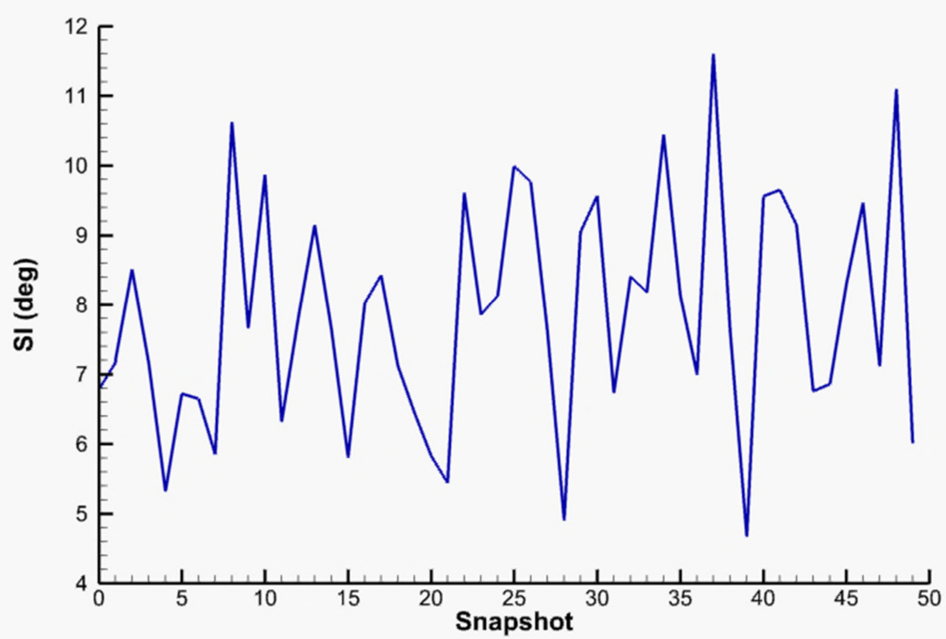

- ❑ Assessment of dynamic distortion
- ❑ Synchronous field data -enables statistics of field descriptor
- ❑ Development of new descriptors

Flow distortion metrics
SI - SC60 maps

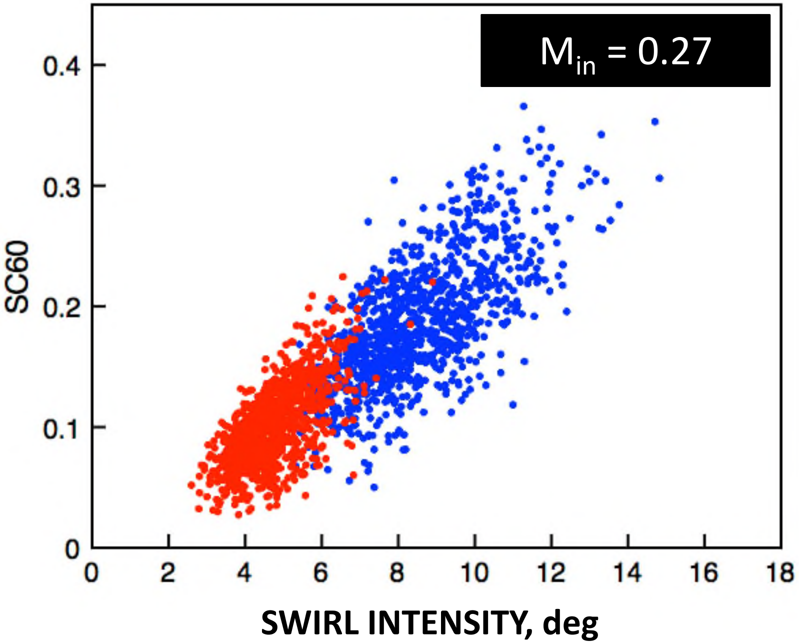

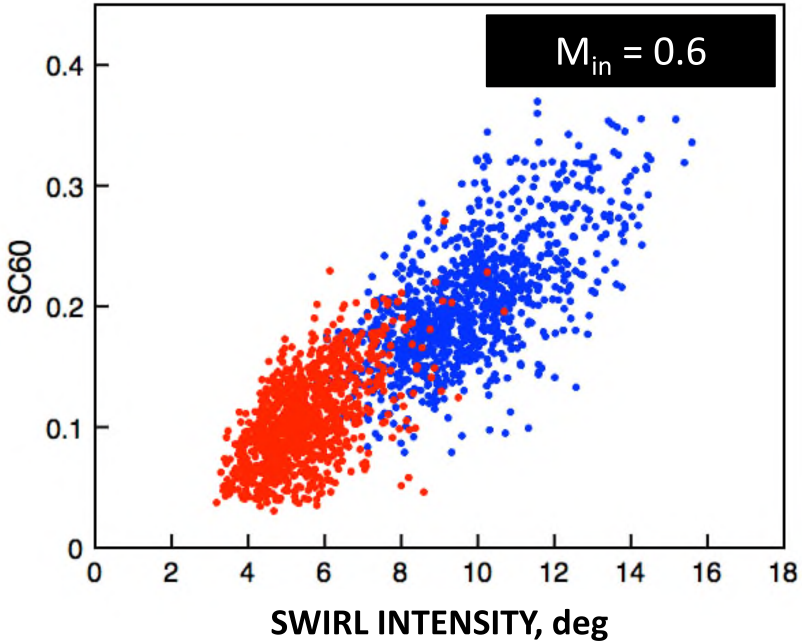

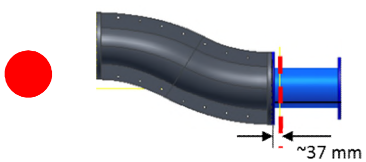

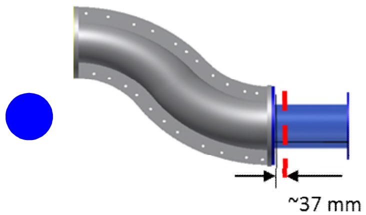

- ❑ Similar distortion signature across Mach number range.

Flow distortion metrics
SAE Swirl pairs

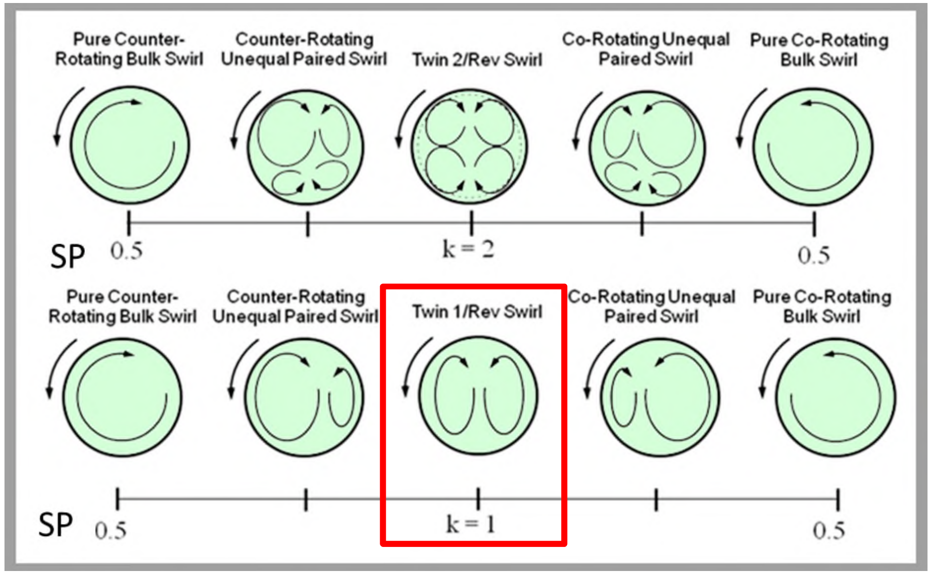

SAE, Report AIR5686

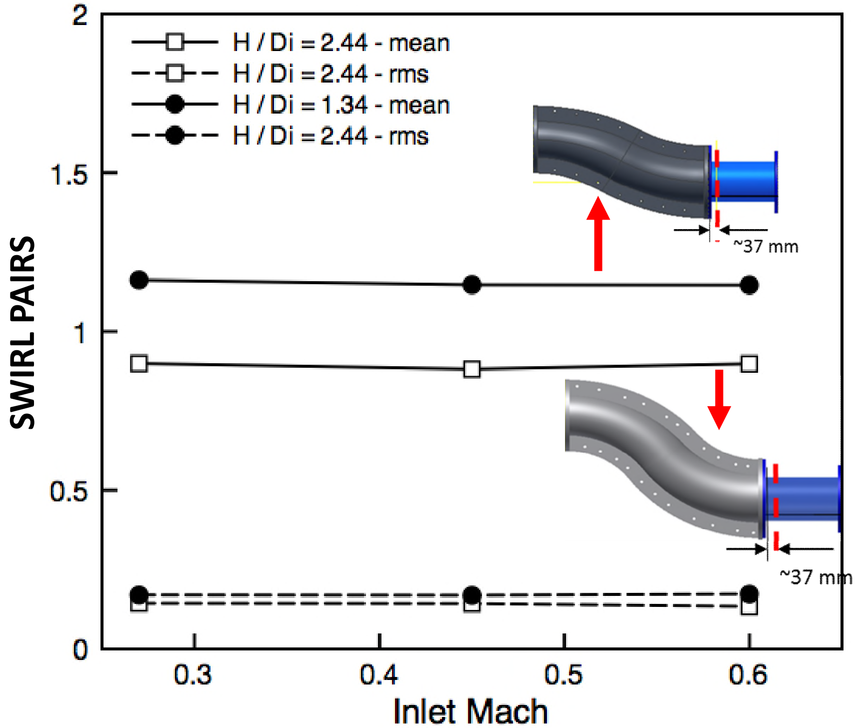

$$SP(i) = \frac{\sum_{k=1}^{m} SS_{i,k}^{+} \cdot \theta_{i,k}^{+} + \sum_{k}^{m} \left| SS_{i,k}^{-} \right| \cdot \theta_{i,k}^{-}}{2 \cdot Max\left\{ SS_{i,k}^{+} \cdot \theta_{i,k}^{+},\ \left| SS_{i,k}^{-} \cdot \theta_{i,k}^{-} \right| \right\}_{k=1,\ldots,m}}$$

Flow distortion metrics
SAE Swirl directivity

Cranfield UNIVERSITY

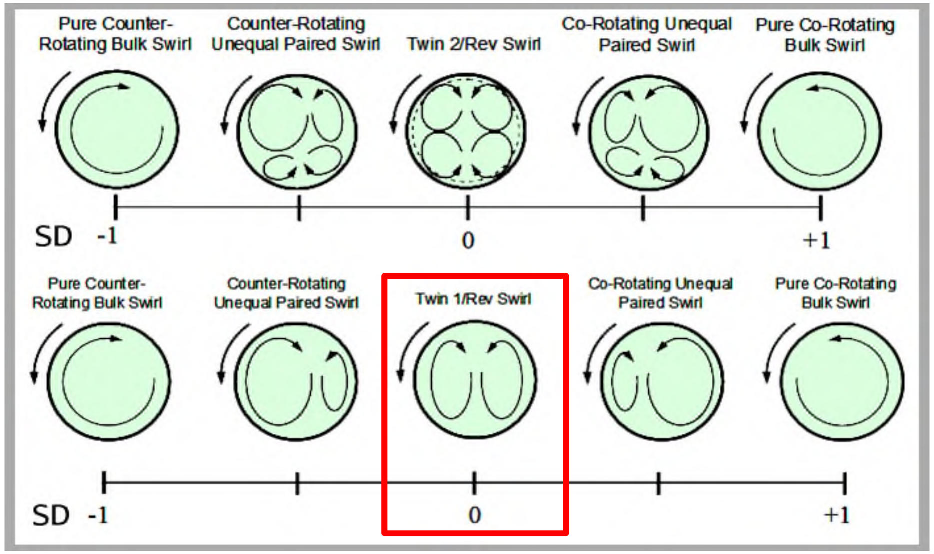

SAE, Report AIR5686

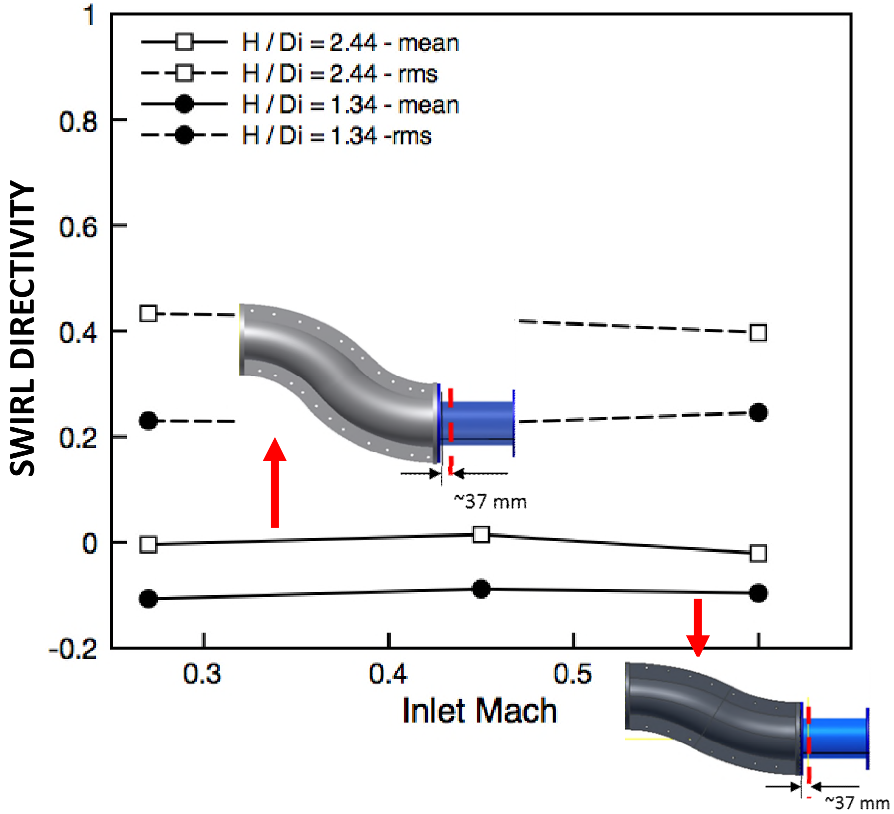

$$SD(i) = \frac{\sum_{k=1}^{m} SS_{i,k}^{+} \cdot \theta_{i,k}^{+} + \sum_{k}^{m} SS_{i,k}^{-} \cdot \theta_{i,k}^{-}}{\sum_{k=1}^{m} SS_{i,k}^{+} \cdot \theta_{i,k}^{+} + \sum_{k}^{m} \left| SS_{i,k}^{-} \right| \cdot \theta_{i,k}^{-}}$$

Flow distortion metrics
SAE SD - SP maps

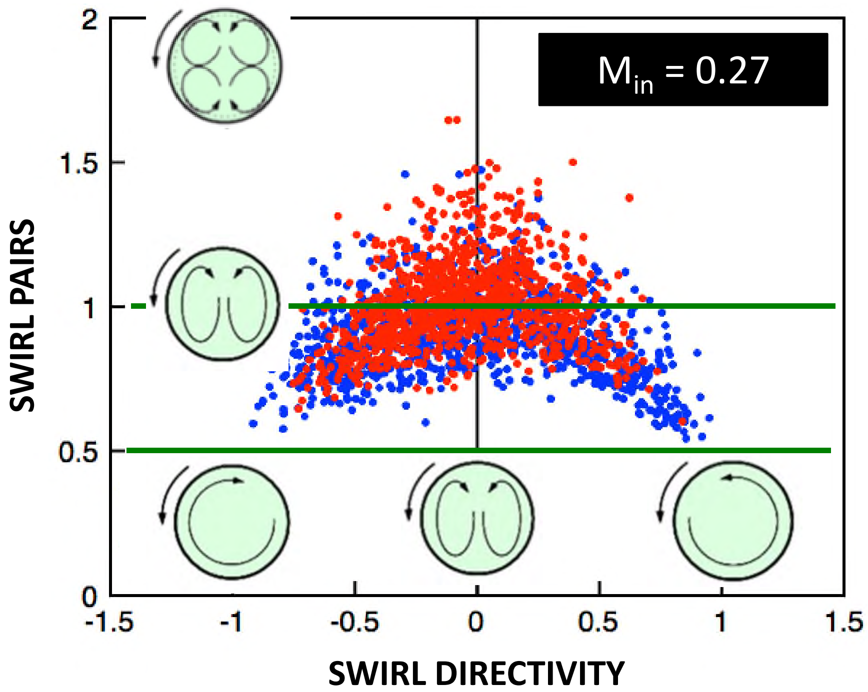

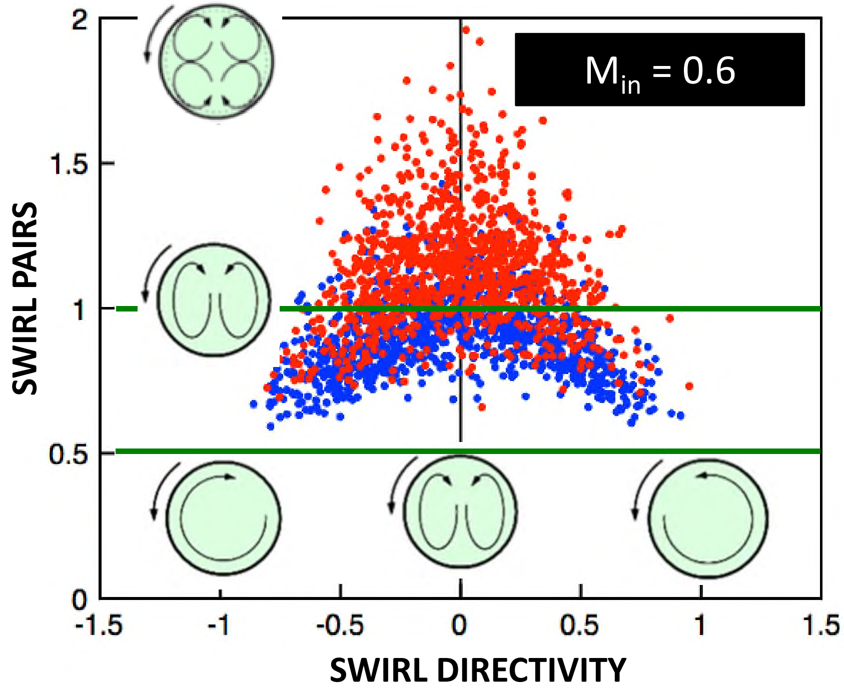

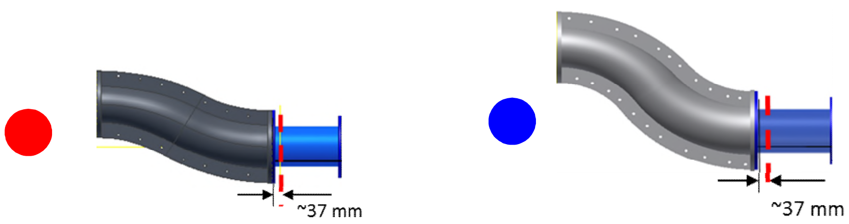

- ❑ Modest Mach number impact.
- ❑ Distortion maps show individuals that deviate from mean behaviour.
- ❑ Identification of extreme events → Stall inception ?

Wrap up

- S-PIV at the cross flow plane at the exit of complex aero engine intakes was enabled and distorted flows were successfully measured.
- **Achieved spatial resolution: 0.8% of the AIP diameter → 9,000 3C velocity vectors across the AIP.** Step change compared to the 40 point measurements across the AIP.
- Unsteady, time averaged and statistical analysis for two S-duct configurations.
- High offset S-duct generates around 80% more distorted and more unsteady flow with higher levels of swirl angle. This is also reflected in the distortion descriptors.
- Mach number has only a modest effect on the AIP flow topology as well in descriptor distribution in both configurations → **Distortion performance dominated mainly by S-Duct offset.**
- Distortion cloud maps allowed the inspection of swirl descriptor distributions in time → Identification of extreme events with potential impact on the downstream compression system.
- **Key step forward in unlocking complex duct aerodynamics.**

Numerical capabilities / DDES / POD

CFD vs experiments I

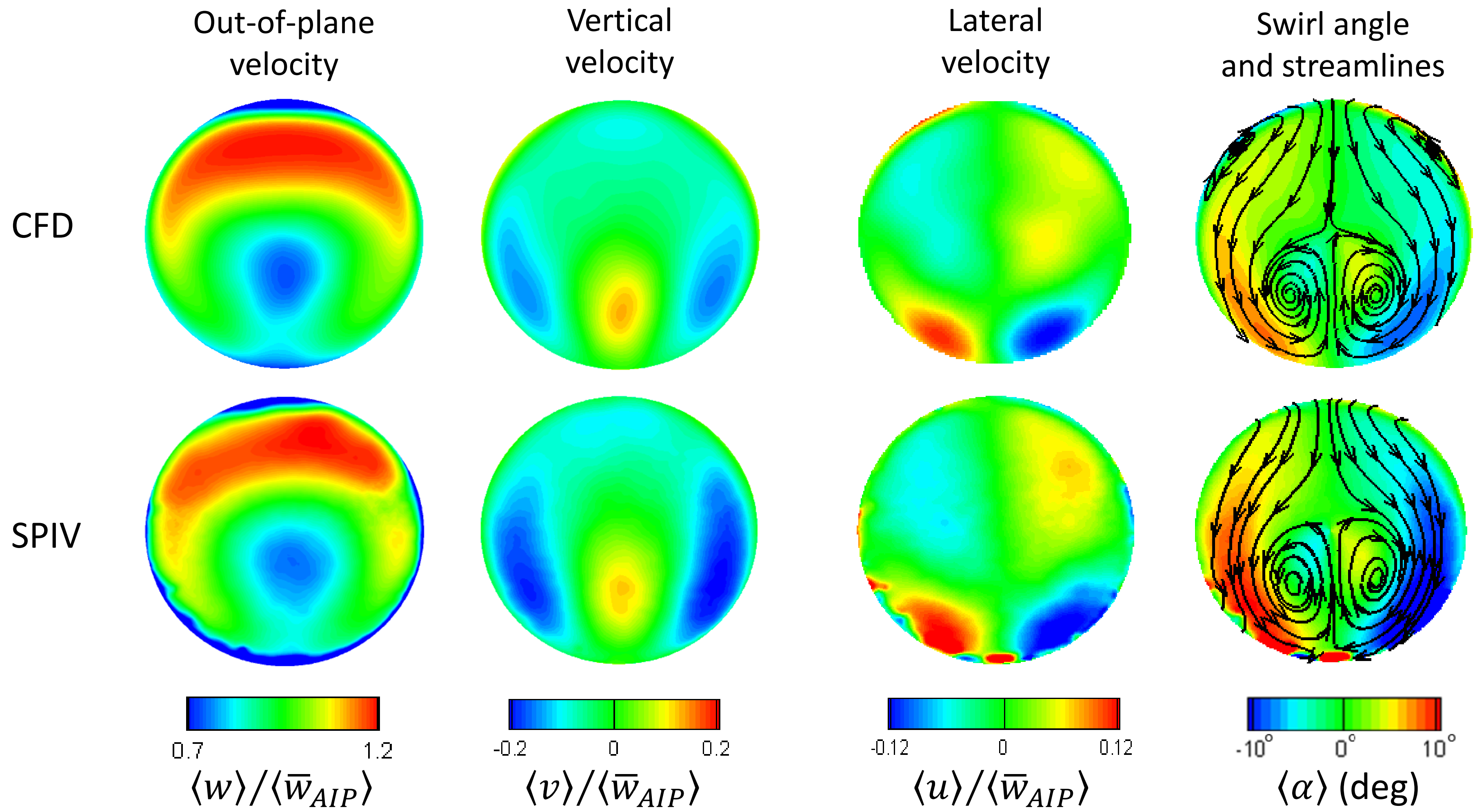

CFD vs experiments II

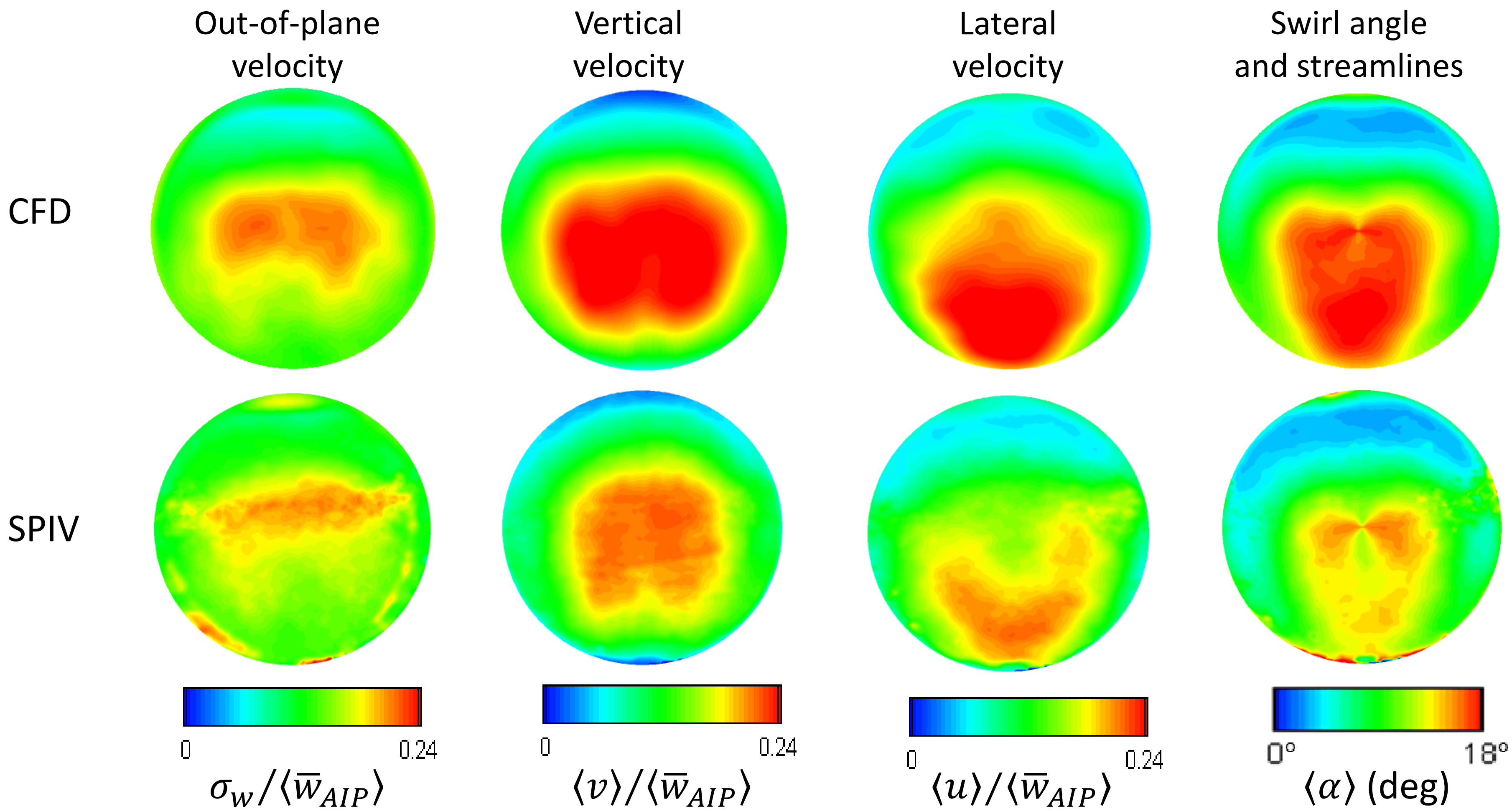

Proper Orthogonal Decomposition (POD)

Cranfield UNIVERSITY

- Coherent structures are obscured by the random flow field
- POD identifies coherent structures ordered by TKE

$$\vec{\boldsymbol{V}}(\vec{\boldsymbol{x}}, \boldsymbol{t}) = \sum_{k=1}^{N} \boldsymbol{a}(\boldsymbol{t})_{\boldsymbol{k}}\, \vec{\emptyset}_{\boldsymbol{k}}(\vec{\boldsymbol{x}})$$

Mode 0

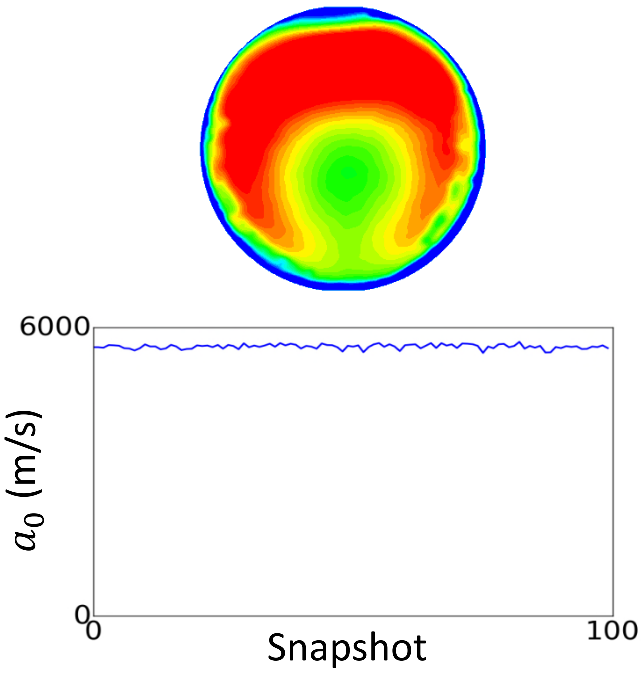

Mode $i > 1$

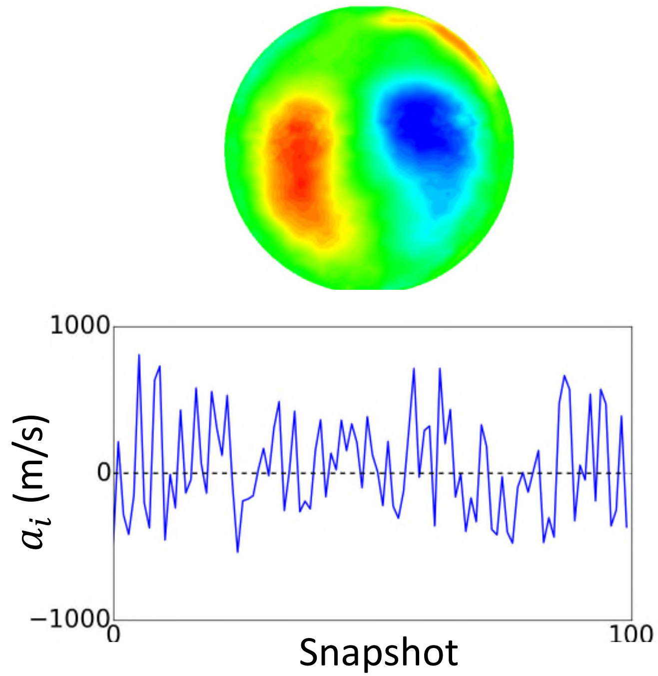

Coherent structure identification via POD – First Switching Mode (FSM)

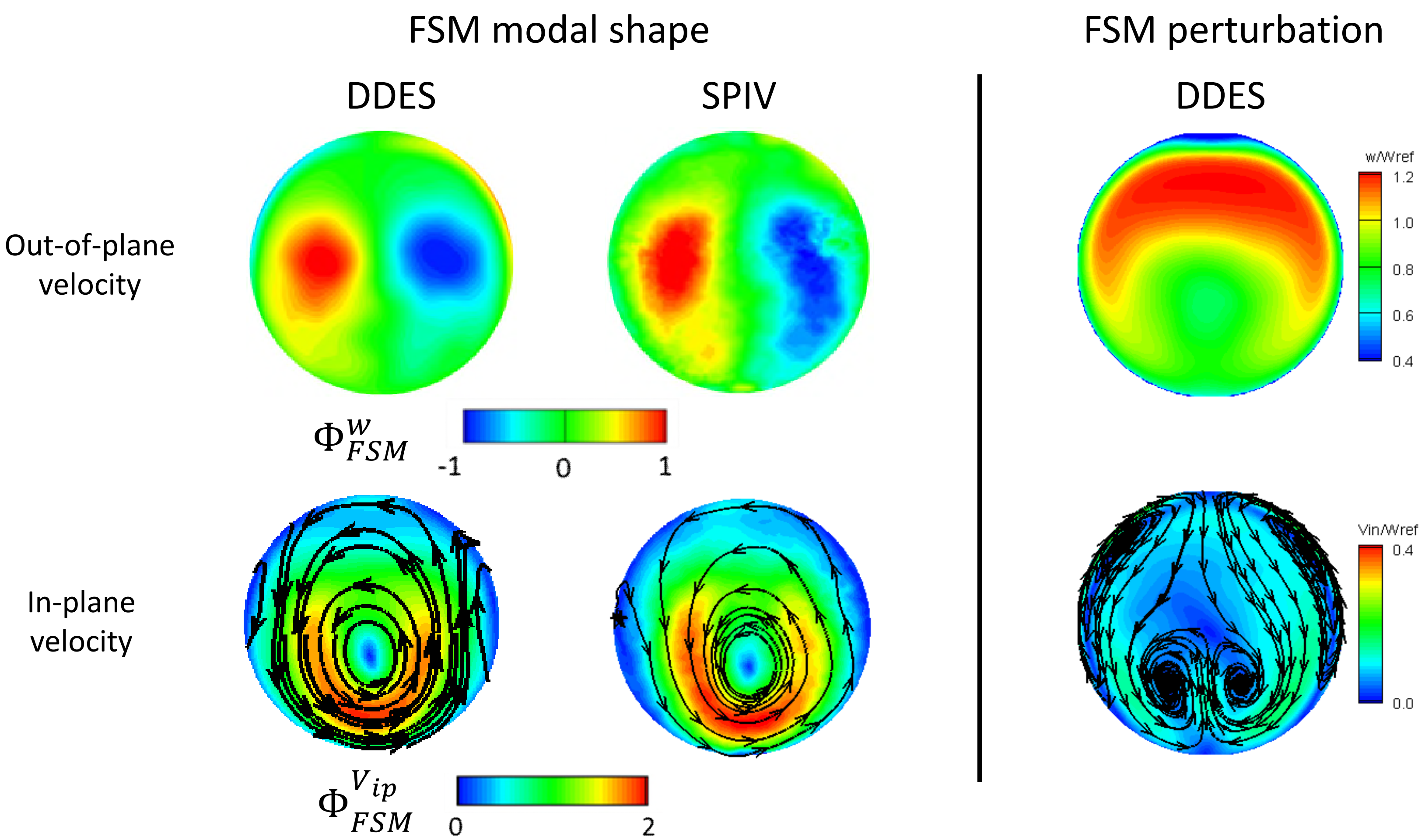

Coherent structure identification via POD – Second Switching Mode (SSM)

SSM modal shape | SSM perturbation

DDES | SPIV | DDES

Out-of-plane velocity

In-plane velocity

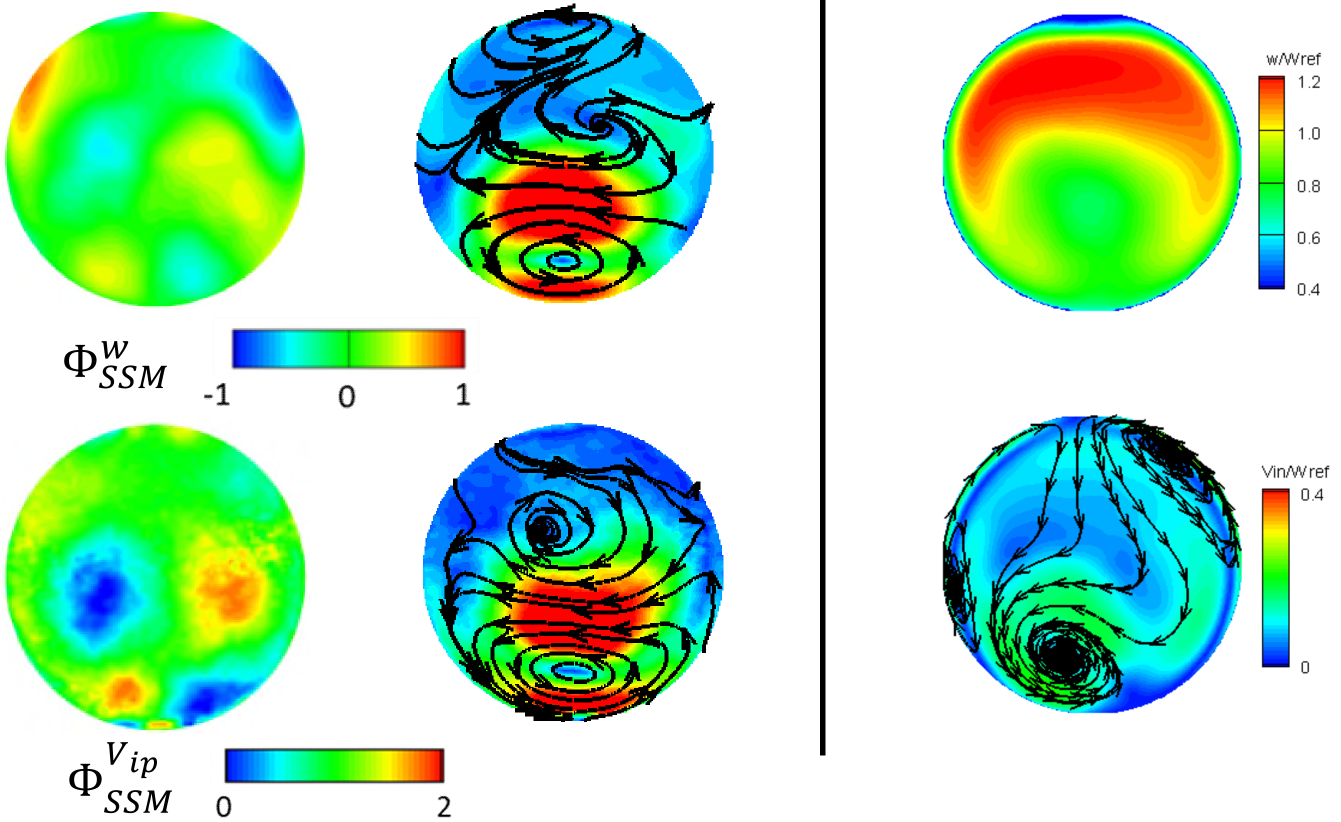

Coherent structure identification via POD – First Vertical Mode (FVM)

FVM modal shape

DDES

SPIV

FVM perturbation

DDES

Out-of-plane velocity

In-plane velocity

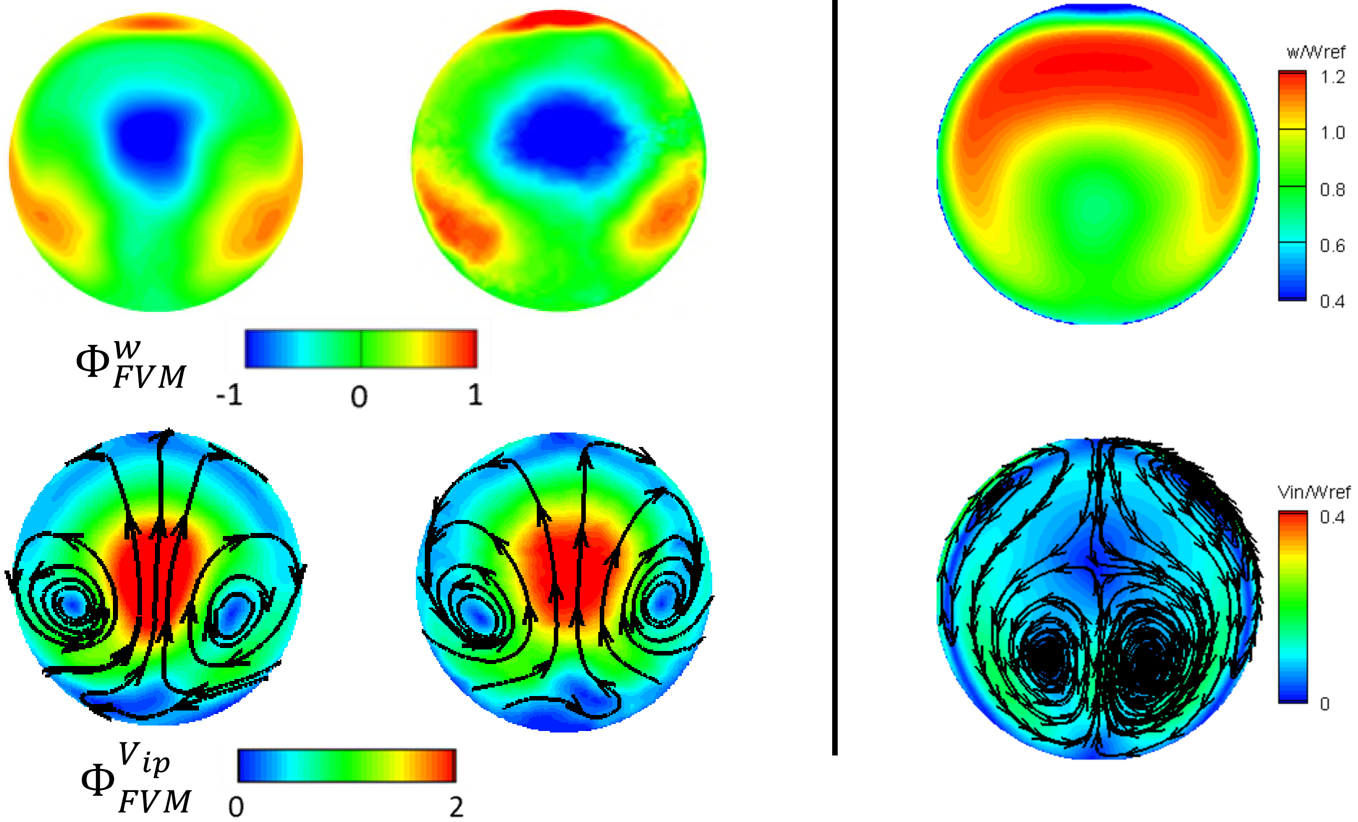

Coherent structure identification via POD – Second Vertical Mode (SVM)

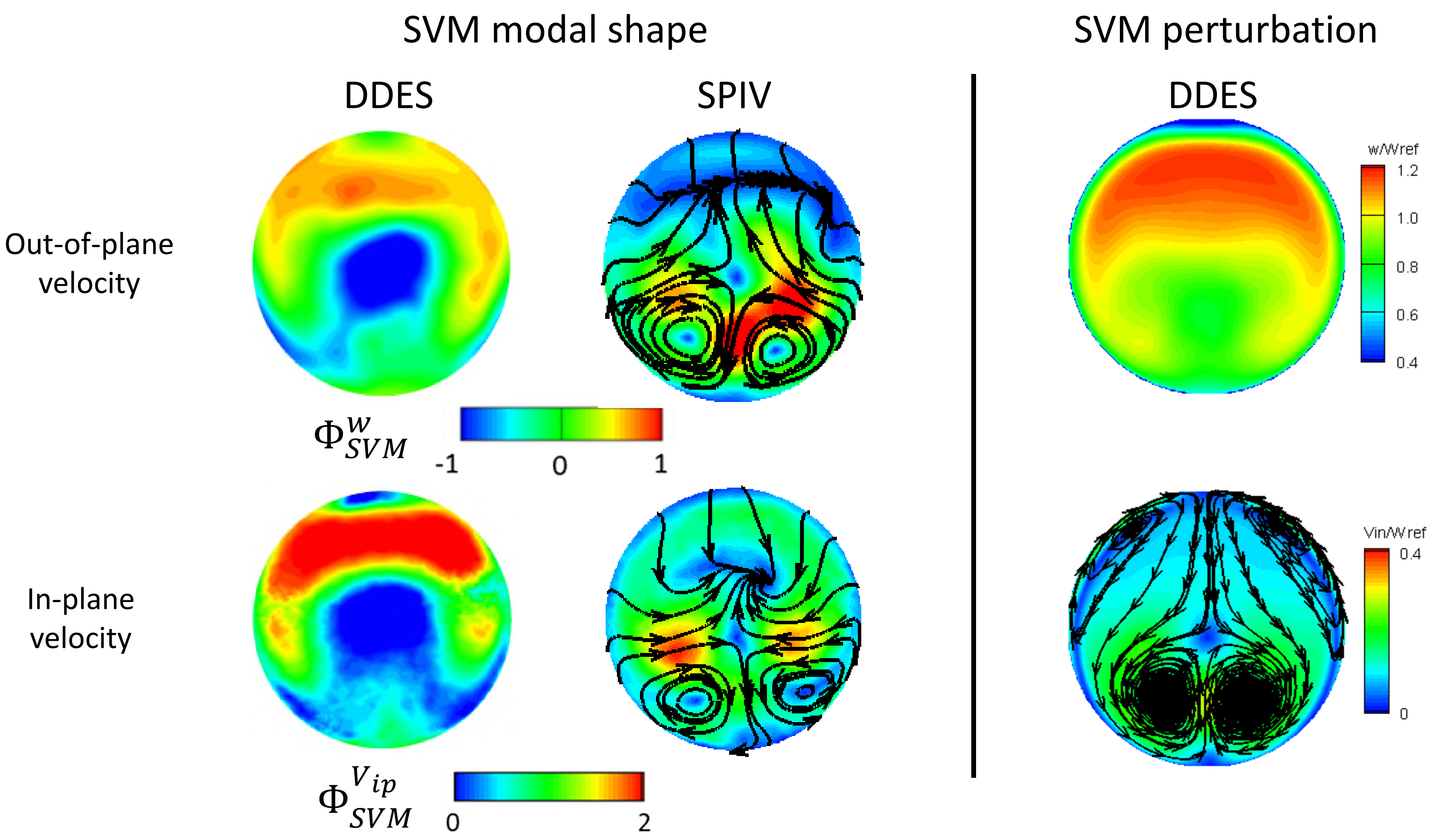

Swirl switching originates from separation region

DDES data only

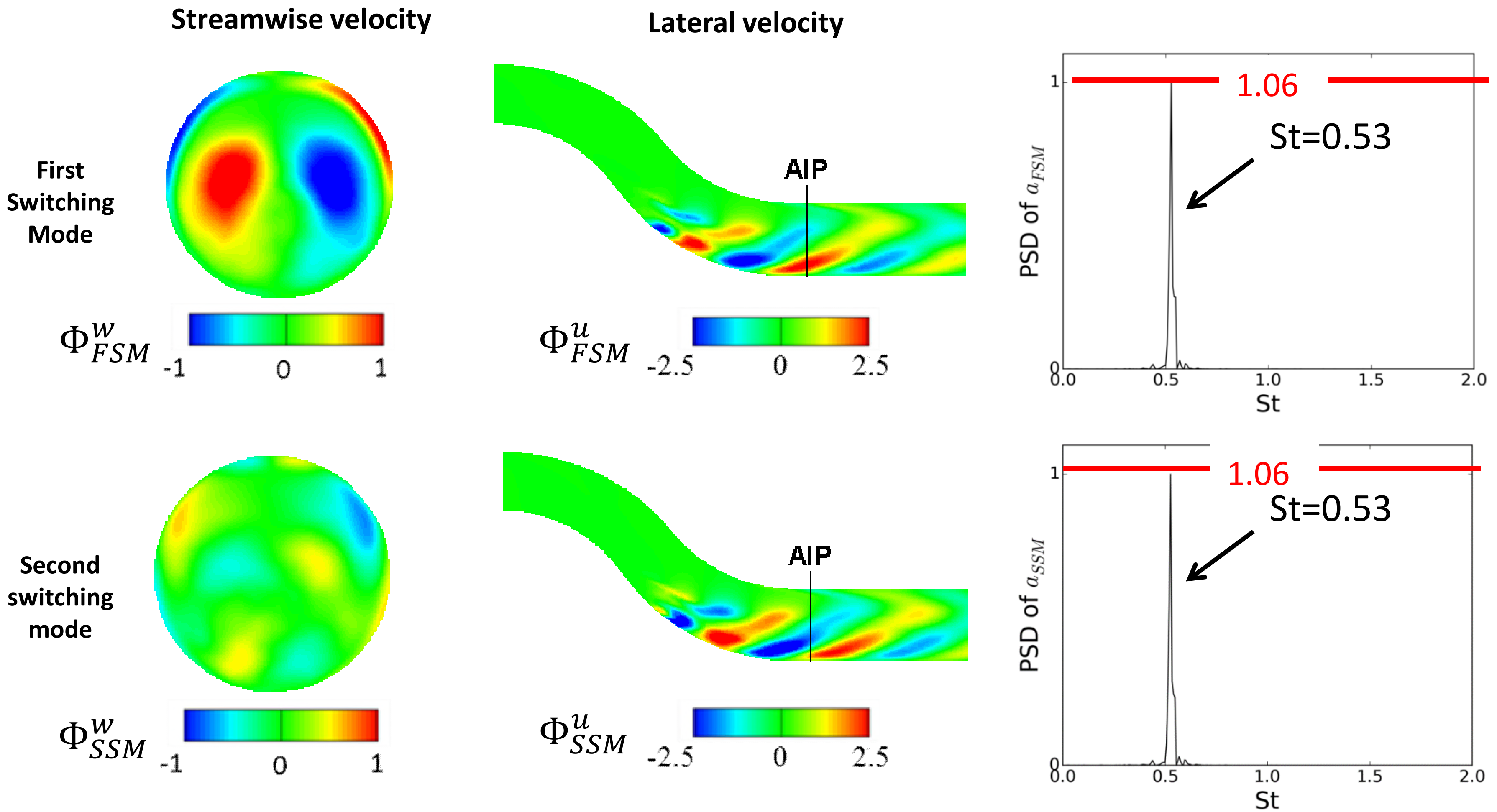

Shear layer unsteadiness

First Vertical Mode

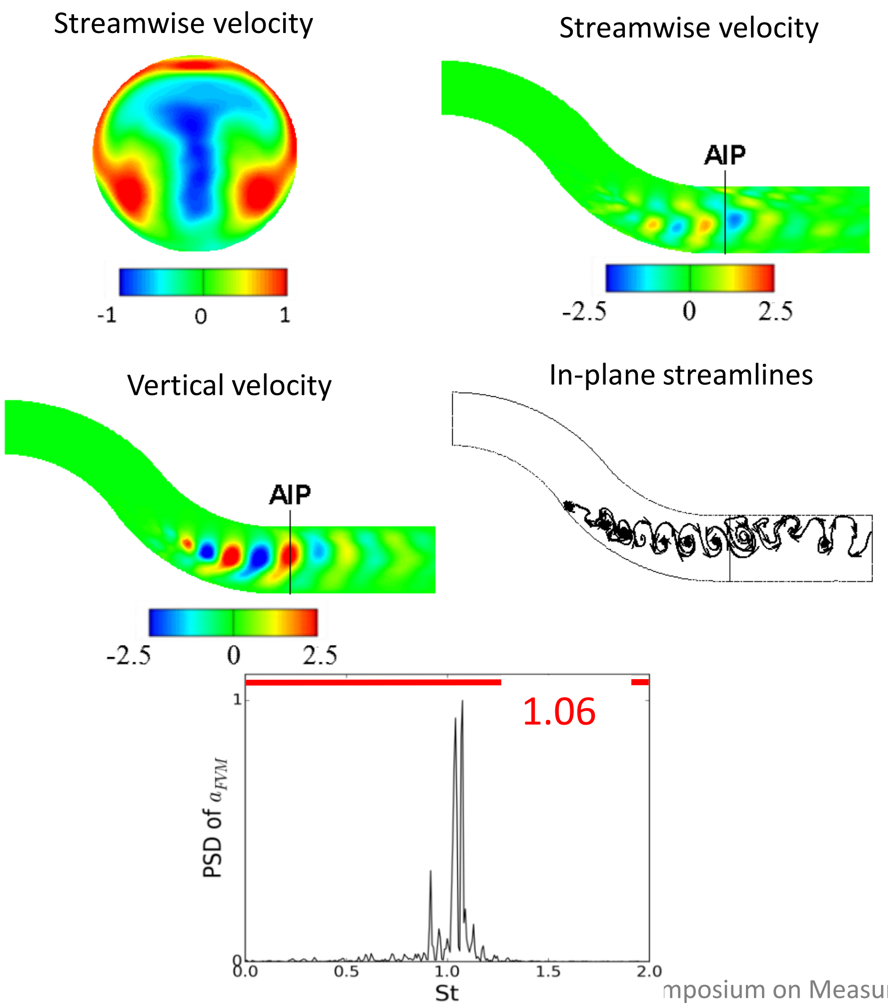

Second Vertical Mode

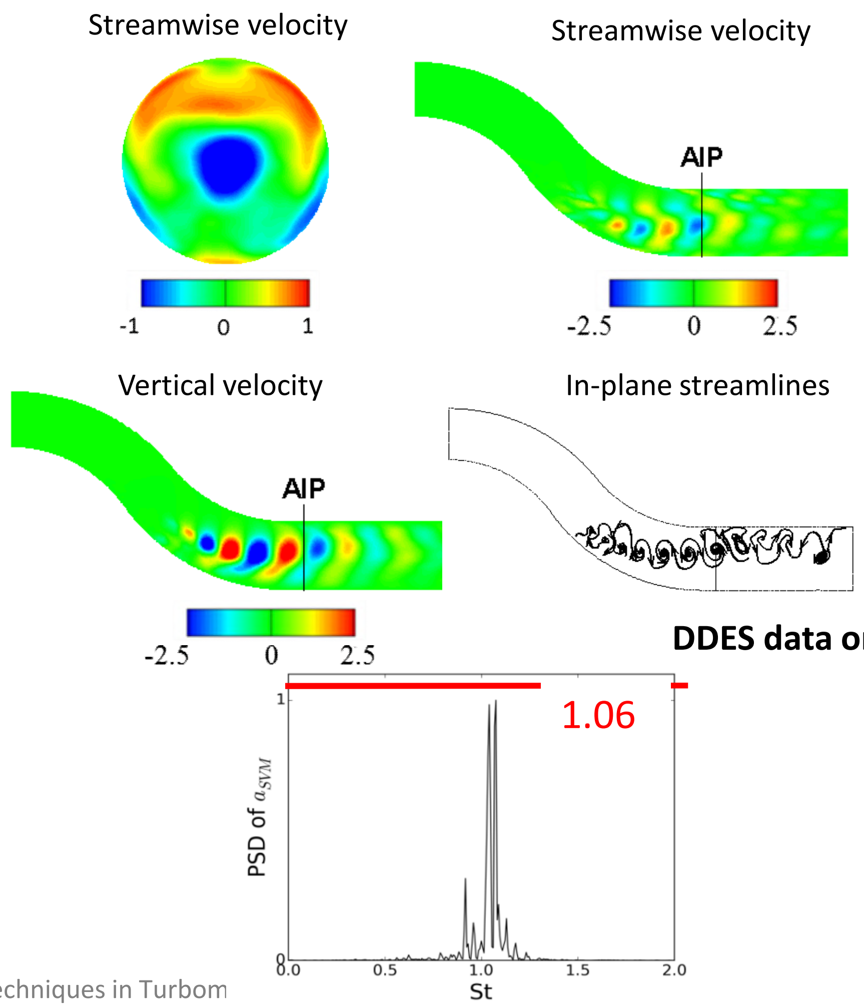

DDES data only

What about inlet pressure distortion ?

Rationale and current challenges

- ❑ Future air vehicles – importance of engine system integration.
- ❑ Compact configurations – sufficient operability margin.
- ❑ Advanced civil configurations - partially embedded engines.

Distributed propulsion

CIVIL

BWB

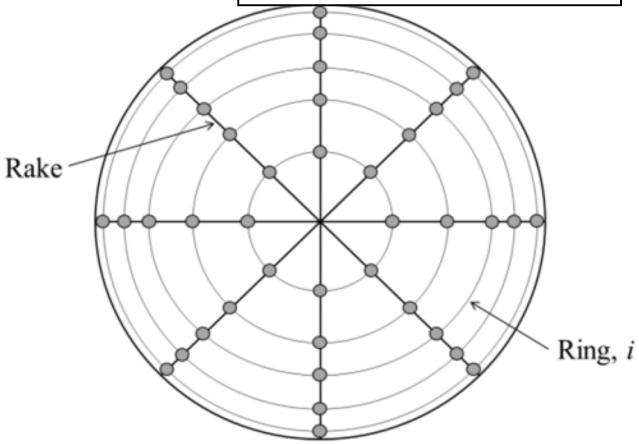

8 x 5 ring and rake AIP discretisation

??

- Poor spatial resolution
- Poor temporal resolution
(most of the times)

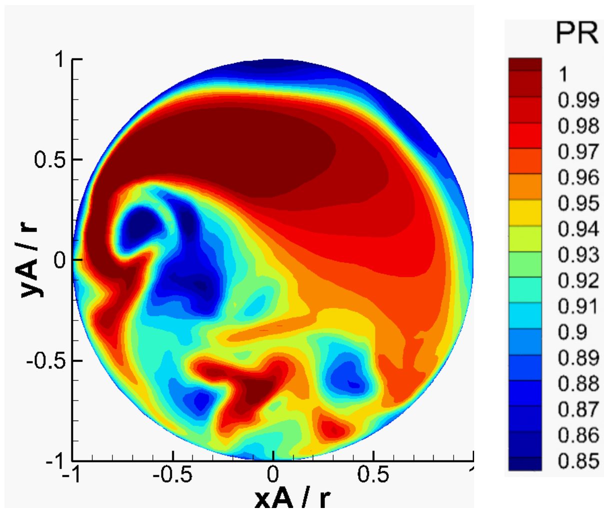

Pressure field from PIV data?

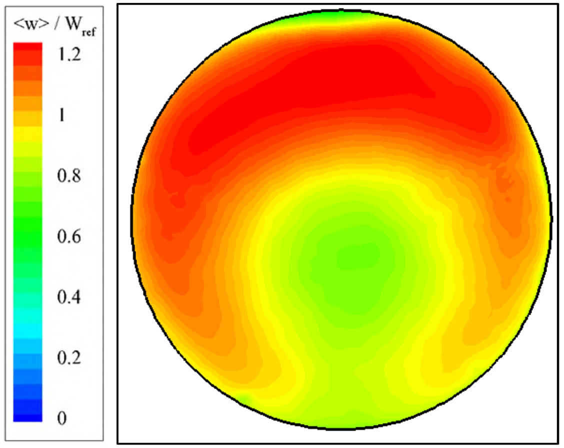

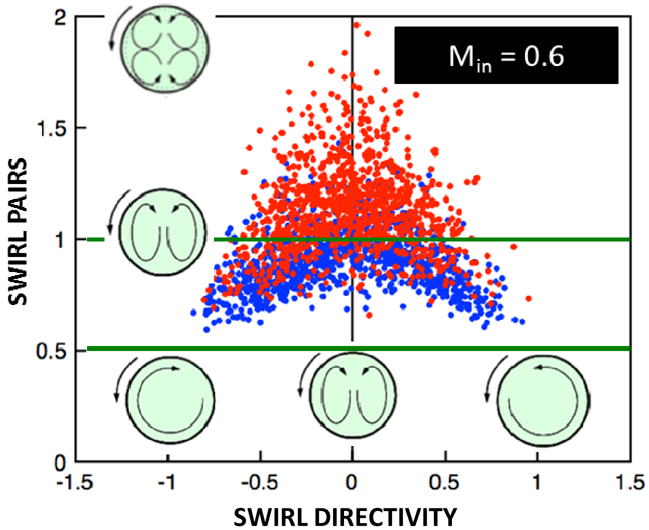

1. Can PIV data be further exploited to determine pressure fields and total pressure distortion metrics ???

2. Planar, tomographic, low bandwidth or time-resolved PIV ???

3. Boundary conditions ???

Pressure derivation from velocity data methods

Cranfield UNIVERSITY

- Integral aerodynamic forces and moments (fluid-structure interactions)
- Velocity field → Pressure field → Mechanical loads (usually measured separately)
- Synchronous estimation of flow kinetics, kinematics and load information
- Time-averaged or time-resolved mode
- Reduce instrumentation needs in wind tunnel tests

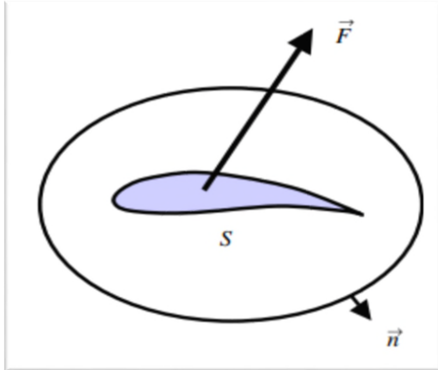

van Oudheusden et al, 2007

$$\mathbf{F}(t) = -\iiint_S \frac{\partial \rho \mathbf{V}}{\partial t}\,\mathrm{d}S - \iint_s \rho(\mathbf{V}\cdot\mathbf{n})\,\mathbf{V}\,\mathrm{d}s + \iint_s (-p\,\mathbf{n} + \boldsymbol{\tau}\cdot\mathbf{n})\,\mathrm{d}s$$

Momentum equation:

$$\underbrace{\nabla p}_{\text{Source}} = \boxed{-\rho\left(\underbrace{\frac{\partial \boldsymbol{u}}{\partial t}}_{\text{Temporal variation}} + \underbrace{\boldsymbol{u}\cdot\nabla\boldsymbol{u}}_{\text{Convection}}\right) + \underbrace{\mu\nabla^2\boldsymbol{u}}_{\text{Viscous diffusion}}}$$

→ Pressure gradient can be derived from velocity data

→ Pressure derived by spatial integration with a static pressure as boundary condition

Pressure derivation from velocity

Momentum equation:

$$\nabla p = -\rho\left(\frac{\partial \boldsymbol{u}}{\partial t} + \boldsymbol{u}\cdot\nabla\boldsymbol{u}\right) + \cancelto{0}{\mu\nabla^2\boldsymbol{u}}$$

$$\begin{cases} \dfrac{\partial p}{\partial r} = -\rho\left(\boxed{\dfrac{\partial u_r}{\partial t}} + \boxed{u_r\dfrac{\partial u_r}{\partial r}} + \boxed{\dfrac{u_\theta}{r}\dfrac{\partial u_r}{\partial \theta}} - \boxed{\dfrac{{u_\theta}^2}{r}} + \boxed{u_z\dfrac{\partial u_r}{\partial z}}\right) \\[2ex] \dfrac{1}{r}\dfrac{\partial p}{\partial \theta} = -\rho\left(\boxed{\dfrac{\partial u_\theta}{\partial t}} + \boxed{u_r\dfrac{\partial u_\theta}{\partial r}} + \boxed{\dfrac{u_\theta}{r}\dfrac{\partial u_\theta}{\partial \theta}} + \boxed{\dfrac{u_\theta u_r}{r}} + \boxed{u_z\dfrac{\partial u_\theta}{\partial z}}\right) \end{cases}$$

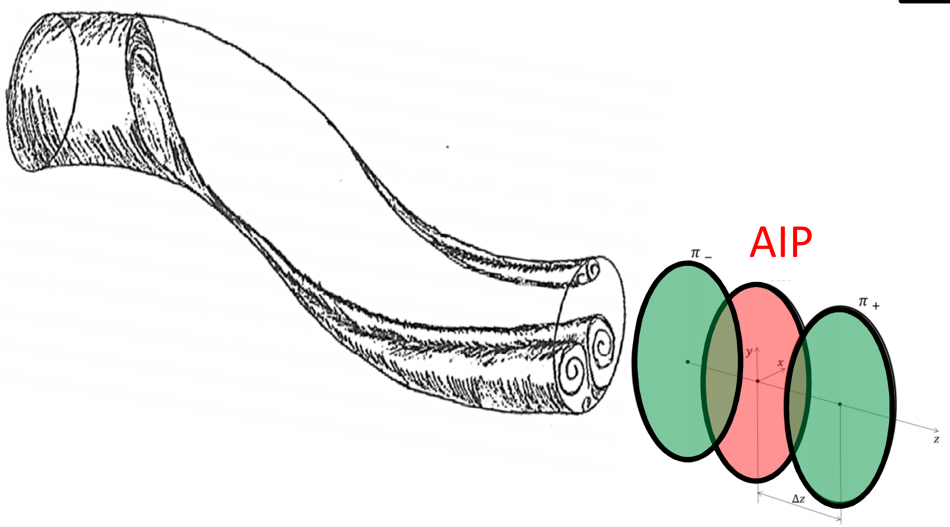

2d-3c low bandwidth S-PIV

Tomo PIV

Time-resolved tomo PIV

Pressure derivation from velocity data - Methods

Cranfield UNIVERSITY

Direct Spatial Integration of momentum equation (DSI):

$$\frac{\partial p}{\partial r} = -\rho\left(\frac{\partial u_r}{\partial t} + u_r\frac{\partial u_r}{\partial r} + \frac{u_\theta}{r}\frac{\partial u_r}{\partial \theta} - \frac{{u_\theta}^2}{r} + u_z\frac{\partial u_r}{\partial z}\right)$$

$$\frac{1}{r}\frac{\partial p}{\partial \theta} = -\rho\left(\frac{\partial u_\theta}{\partial t} + u_r\frac{\partial u_\theta}{\partial r} + \frac{u_\theta}{r}\frac{\partial u_\theta}{\partial \theta} + \frac{u_\theta u_r}{r} + u_z\frac{\partial u_\theta}{\partial z}\right)$$

with

$$\rho_{i,j} = \frac{p_{i,j}}{Rt}$$

$$t = t_0 - \frac{1}{2}\frac{u_{i,j}^2}{c_p}$$

Numerical method as in *Baur et al.*, 1999

Poisson Pressure Equation (PPE):

$$\nabla^2 p = -\rho\nabla\cdot\left[\frac{d\boldsymbol{u}}{dt} + \boldsymbol{u}\cdot\nabla\boldsymbol{u}\right] = \frac{1}{r}\frac{\partial}{\partial r}\left(r\frac{\partial p}{\partial r}\right) + \frac{1}{r^2}\frac{\partial^2 p}{\partial \theta^2} + \frac{\partial^2 p}{\partial z^2} =$$

$$= -\rho\left[\frac{1}{r}\frac{\partial u_r}{\partial t} + \frac{\partial^2 u_r}{\partial r\partial t} + \frac{1}{r}\frac{\partial^2 u_\theta}{\partial \theta\partial t} + \frac{\partial^2 u_z}{\partial z t}\right]$$

$$-\rho\left[\left(\frac{\partial u_r}{\partial r}\right)^2 + \frac{1}{r^2}\left(\frac{\partial u_\theta}{\partial \theta}\right)^2 + \left(\frac{\partial u_z}{\partial z}\right)^2 + \frac{2}{r}\frac{\partial u_\theta}{\partial r}\frac{\partial u_r}{\partial \theta}\right.$$

$$+2\frac{\partial u_z}{\partial r}\frac{\partial u_r}{\partial z} + \frac{2}{r}\frac{\partial u_z}{\partial \theta}\frac{\partial u_\theta}{\partial z} + \left(\frac{u_r}{r}\right)^2 - 2\frac{u_\theta}{r}\frac{\partial u_\theta}{\partial r}$$

$$\left.+2\frac{u_r}{r^2}\frac{\partial u_\theta}{\partial \theta}\right]$$

Numerical method as in *Anderson*, 1995

- ❑ Impact of flow density
- ❑ Impact of out-of-plane velocity gradients
- ❑ Impact of temporal velocity gradients
- ❑ Impact of boundary condition

Pressure derivation from velocity data – Boundary conditions

Cranfield UNIVERSITY

DSI

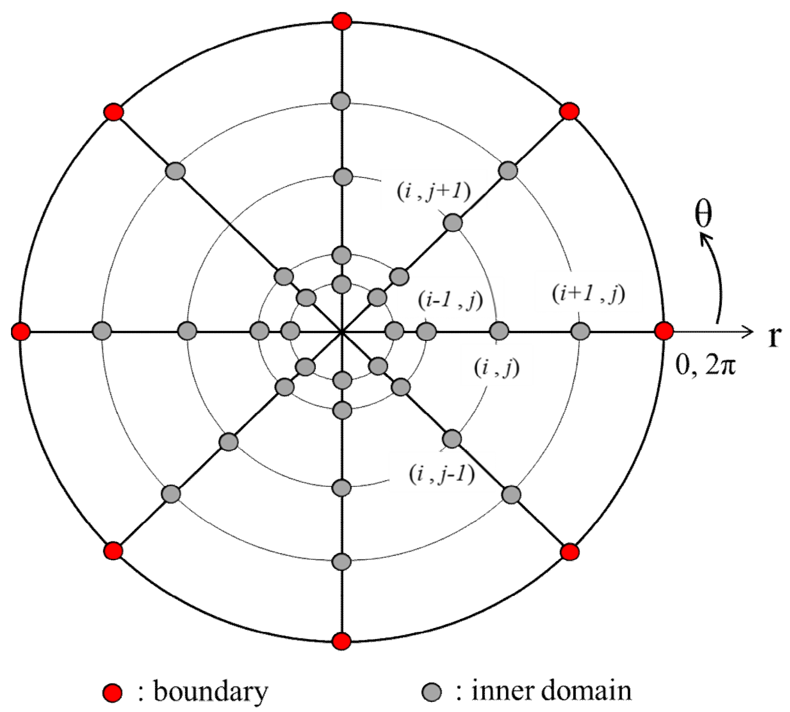

- ❑ Static pressure along outer boundary

PPE

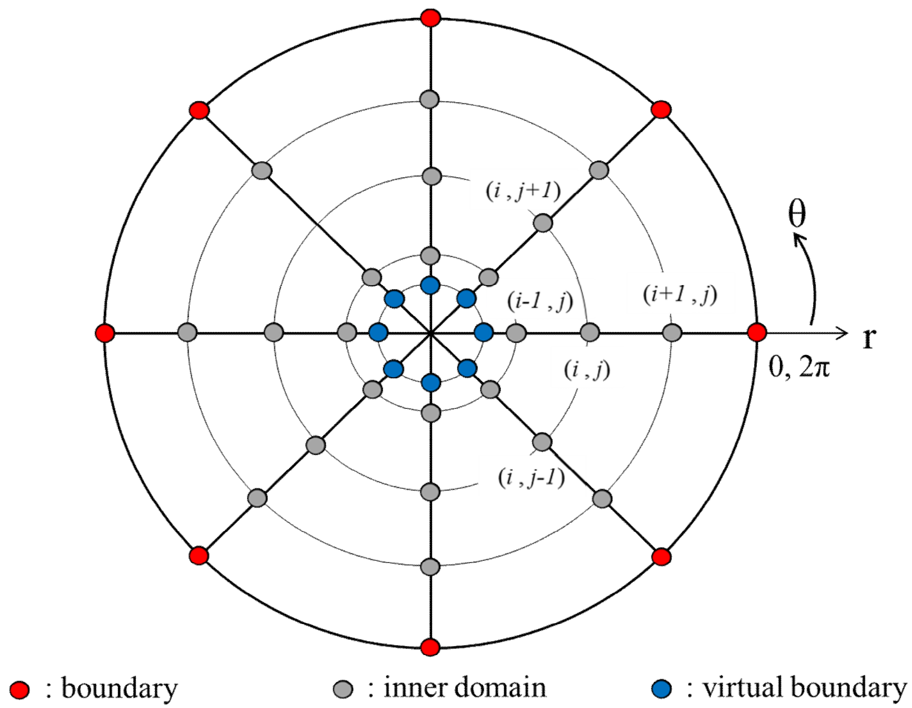

- ❑ Static pressure along outer boundary
- ❑ Divergence of static pressure along virtual boundary

Agenda

METHOD VERIFICATION

S-duct configuration & verification data

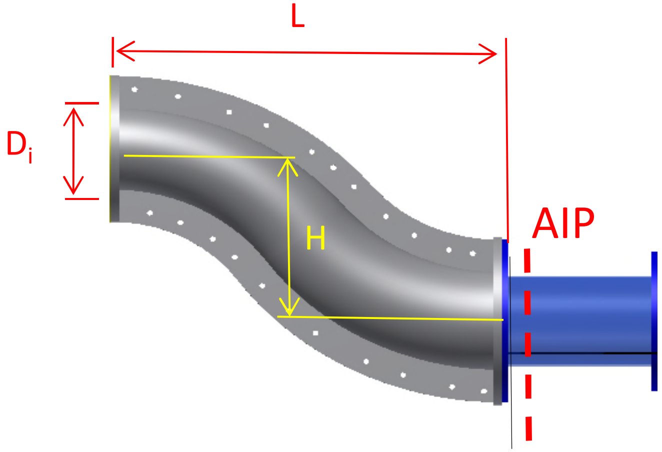

	Inlet Mach	Inlet Re_D
D_i = 121.6 mm	0.27	6.01e+5
A_{out} / A_{in} = 1.52	0.45	10.05e+5
H / D_i = 2.44	0.6	13.8e+5
L / D_i = 4.95		Presented here

Computational methods:

1. RANS with k-ω SST
2. Delayed Detached Eddy Simulations with Δt=6 µs or $\Delta t/t_c$ = 0.00175
3. Velocity field extracted from CFD - mapped onto a uniform 50 x 180 points polar grid
4. 200 boundary points equi-spaced circumferentially

…further details on CFD methods in ***MacManus et al*, AIAA-2015-3304**

Time averaged pressure reconstruction–
Direct Spatial Integration (DSI)

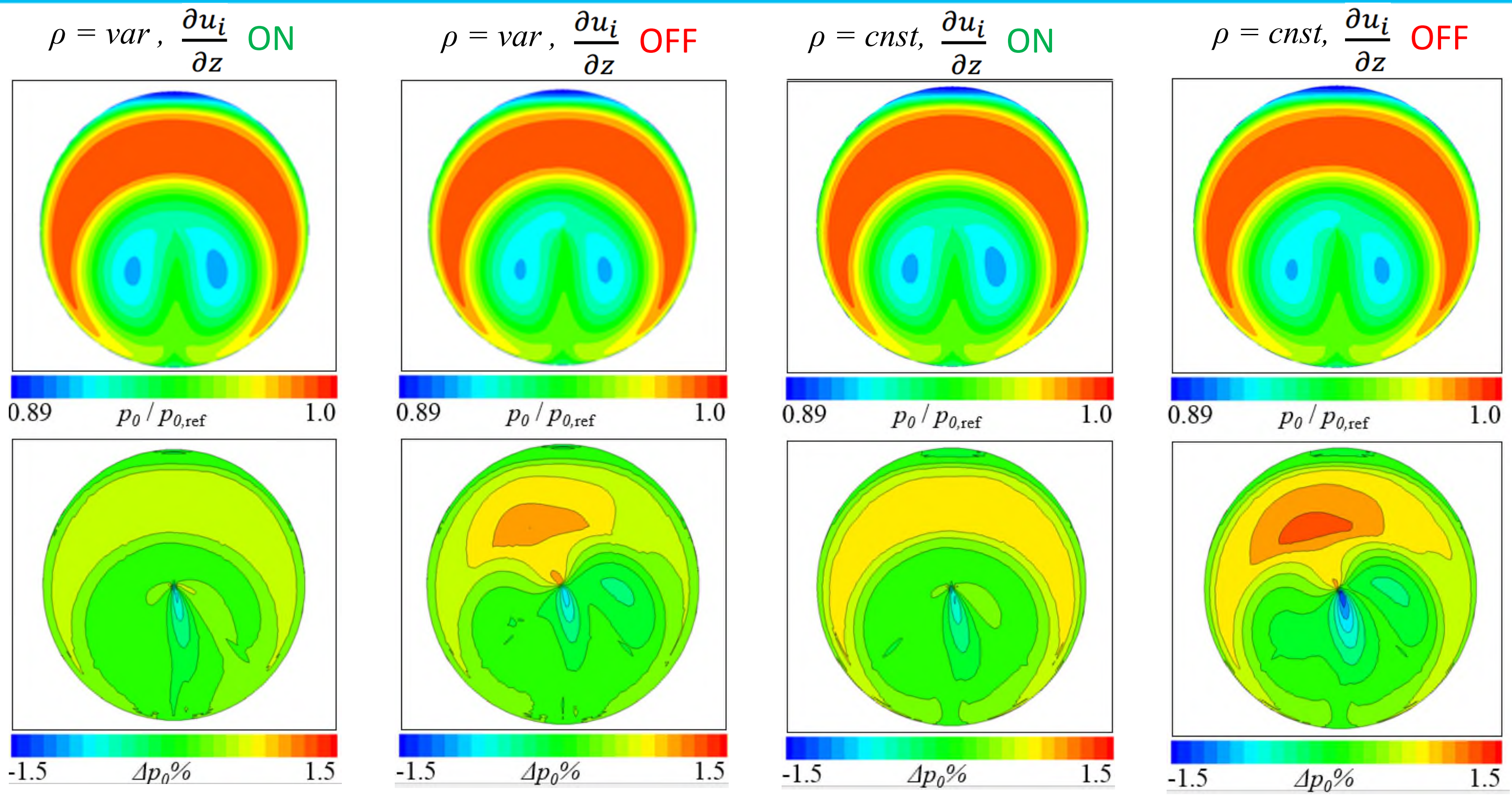

Departure ±0.7% | Departure ±1% | Departure ±1.2% | Departure ±1.5%

Time averaged pressure reconstruction–
Poisson Pressure Equation (PPE)

$\rho = var\ ,\ \frac{\partial u_i}{\partial z}$ ON

$\rho = var\ ,\ \frac{\partial u_i}{\partial z}$ OFF

$\rho = cnst,\ \frac{\partial u_i}{\partial z}$ ON

$\rho = cnst,\ \frac{\partial u_i}{\partial z}$ OFF

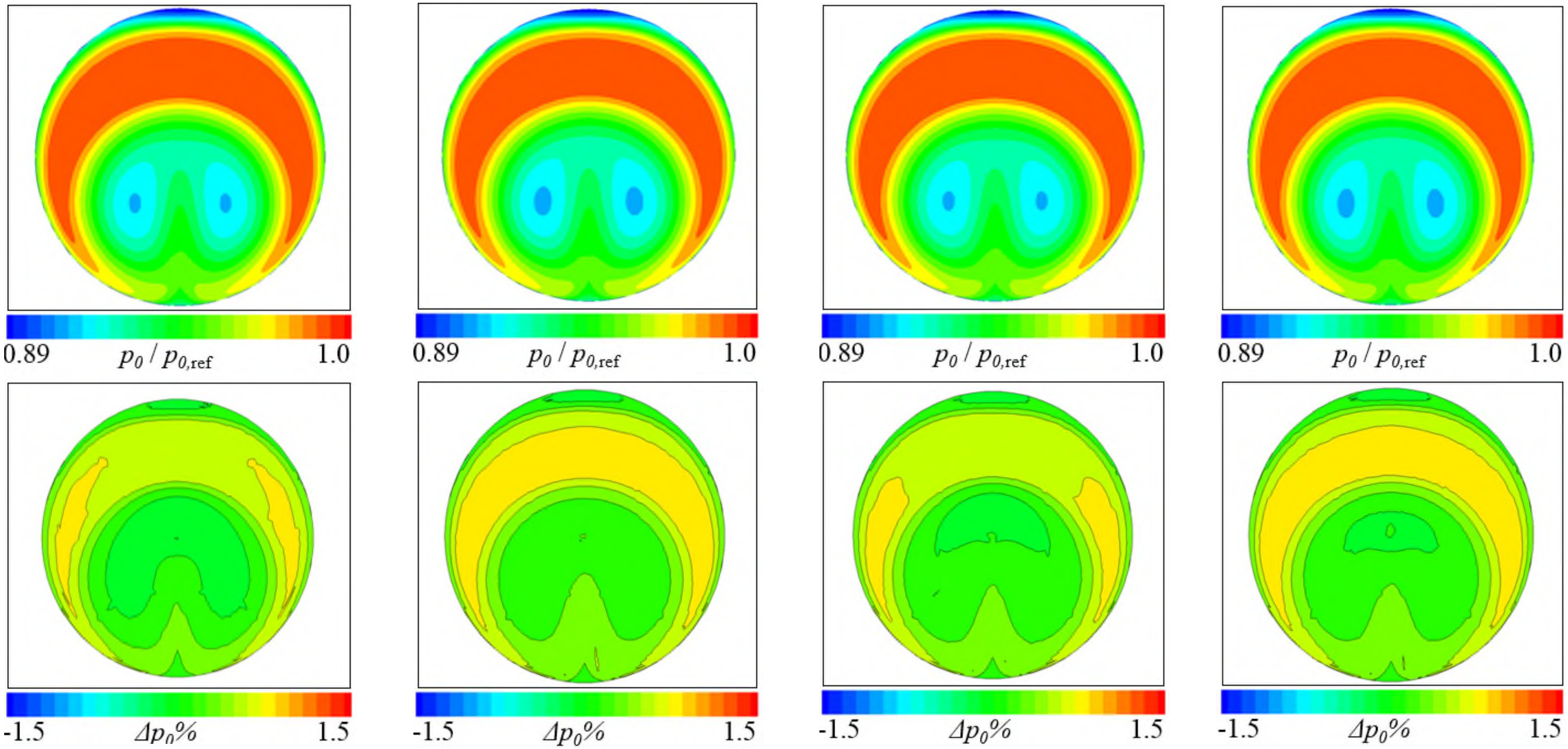

Departure +1.1%

Departure +1.1%

Departure +1.1%

Departure +1.1%

Time averaged pressure reconstruction

	DENSITY	$\left(\frac{\partial u_i}{\partial z}\right)$	$Ix10^3$ M_{in}=0.6	$Ix10^3$ M_{in}=0.27
DSI	variable	on	6.7	6.4
	variable	off	15	16
	constant	on	6.8	6.5
	constant	off	15	17
PPE	variable	on	5.3	5.5
	variable	off	5.6	6.5
	constant	on	5	5.5
	constant	off	4.8	6.5

Method accuracy index:

$$I = \frac{\sqrt{\frac{\sum_{i=1}^{n_r}\sum_{j=1}^{m_\theta}(p_{rec}-p_{CFD})^2}{n_r \cdot m_\theta}}}{q}$$

- ❑ DSI accuracy affected by out-of-plane velocity terms
- ❑ Density has no major impact
- ❑ PPE provides slightly better reconstruction accuracy
- ❑ PPE accuracy constant regardless of density of out-of-plane velocity gradients treatment
- ❑ Both methods allow reasonably accurate derivation of pressure fields from steady, planar, 3C velocity data

Unsteady pressure reconstruction– Direct Spatial Integration (DSI)

Cranfield UNIVERSITY

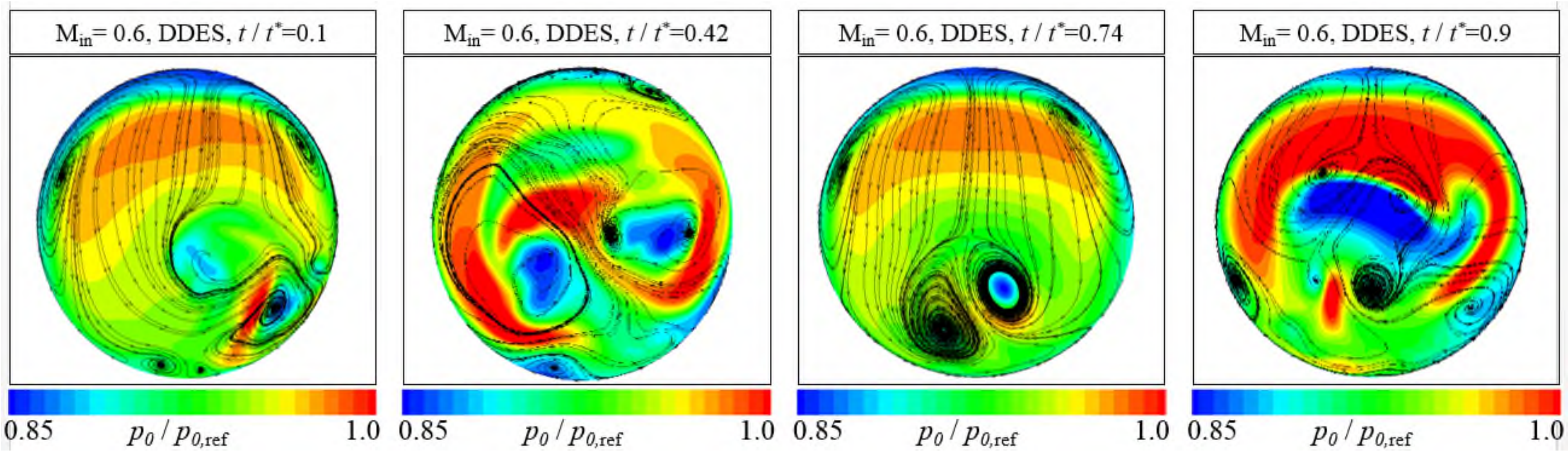

- Delayed Detached Eddy Simulations (k-ω SST)
- Δt=6 μs or $\Delta t/t_c$ = 0.00175
- Convective time t_c = 3.41 ms
- Solution saved every 3 timesteps or 18 μs

Unsteady pressure reconstruction– Direct Spatial Integration (DSI)

$\rho = var\,,\ \frac{\partial u_i}{\partial z}$ ON , $\frac{\partial u_i}{\partial t}$ ON

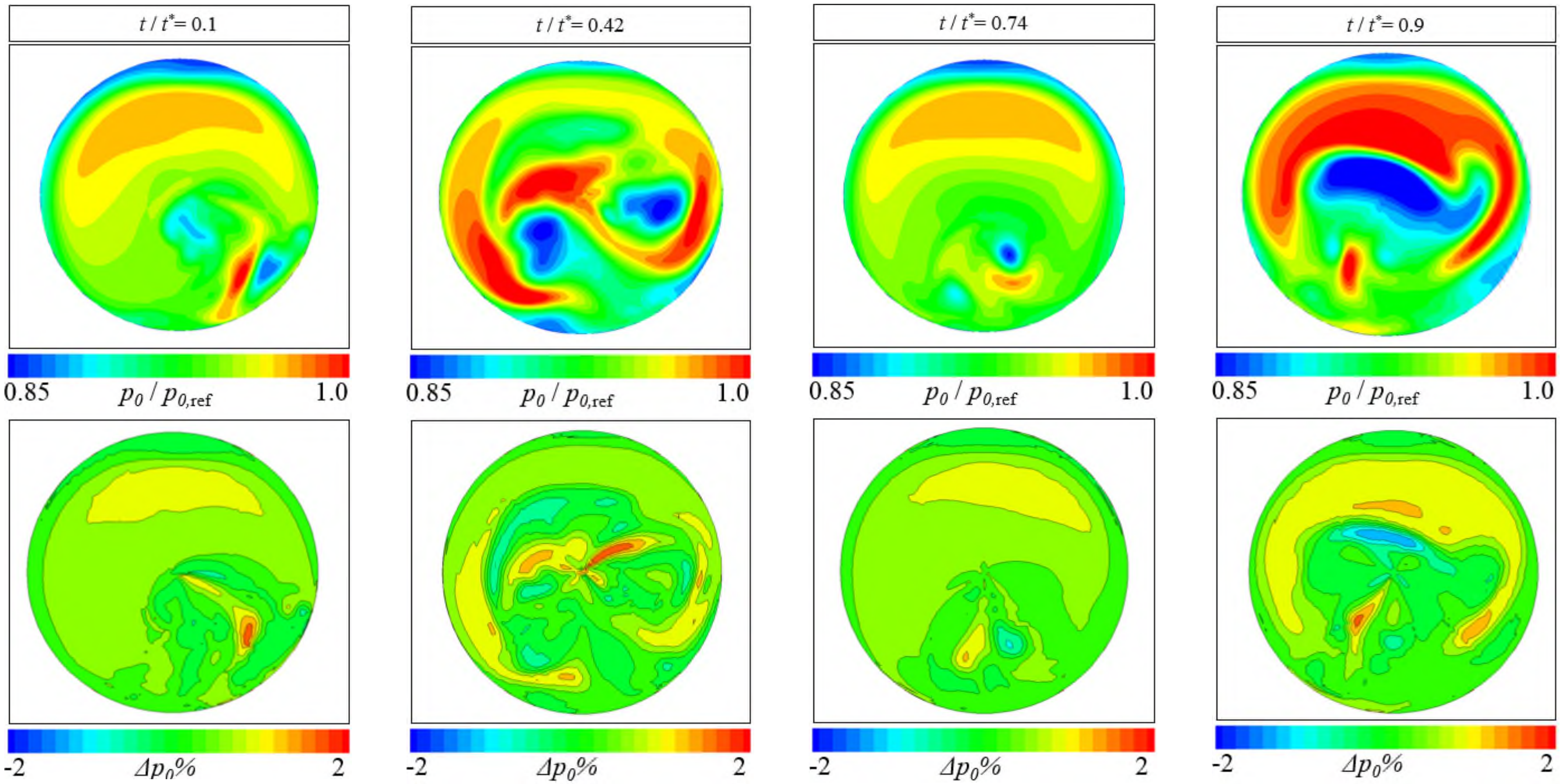

- Highly distorted, unsymmetrical instantaneous flow fields
- DSI robust and accurate enough to reconstruct pressure fields (departure ±1.5%)

Unsteady pressure reconstruction– Direct Spatial Integration (DSI)

$\rho = var$, $\frac{\partial u_i}{\partial z}$ OFF , $\frac{\partial u_i}{\partial t}$ OFF

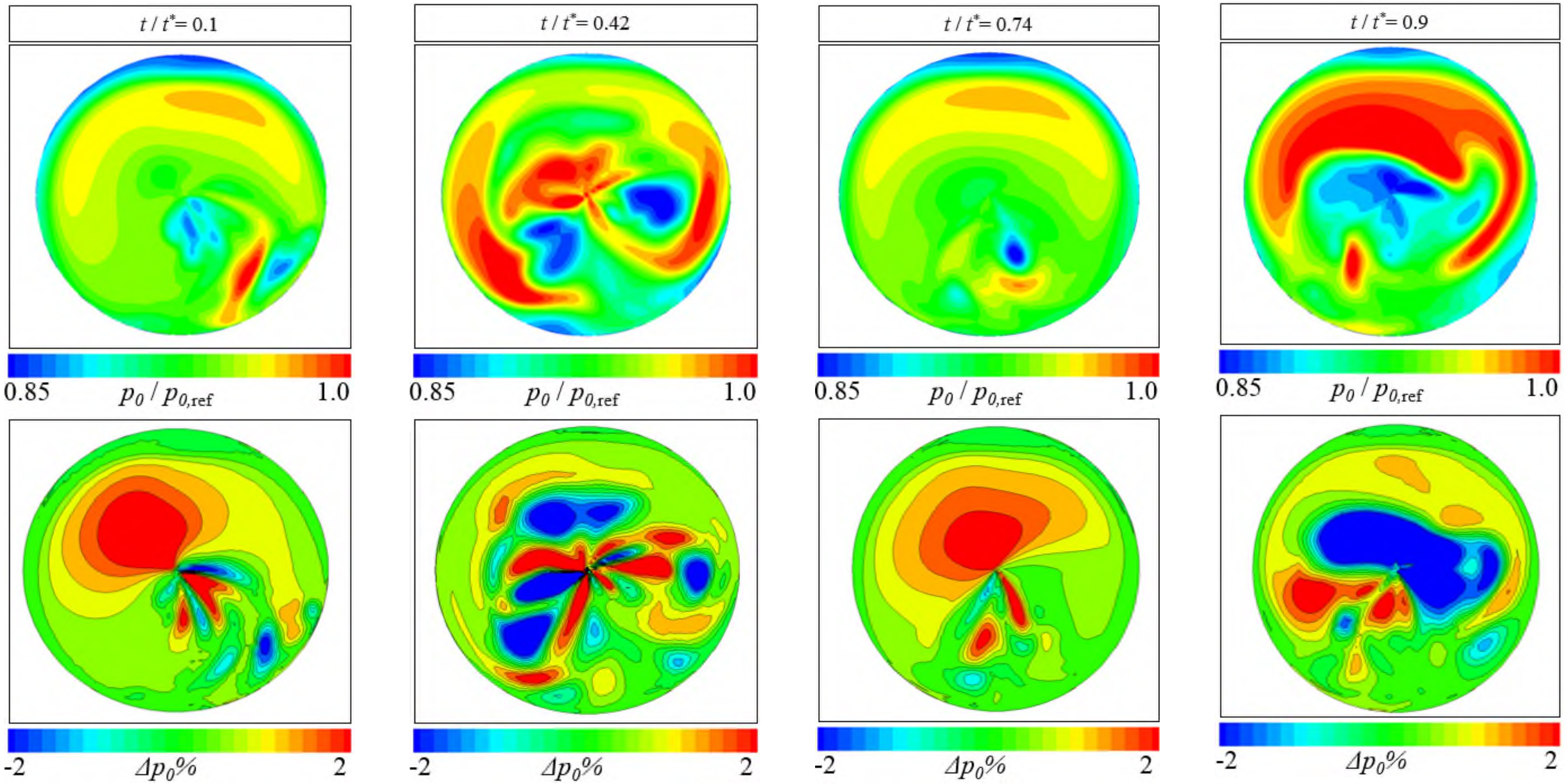

- Accuracy penalty (departure ±8%)

Total pressure distortion descriptors

$$CDI = \mathrm{Max}_{i=1}^{n_{radius}-1}\left(0.5\left[\frac{p_{0,i}-p_{0,min_i}}{p_{0,avg}}+\frac{p_{0,i+1}-p_{0,min_{i+1}}}{p_{0,avg}}\right]\right)$$

$$RDI = \mathrm{Max}\left(\frac{p_{0,avg}-p_{0,inner\ ring}}{p_{0,avg}},\frac{p_{0,avg}-p_{0,outer\ ring}}{p_{0,avg}}\right)$$

$$DC(60) = \frac{p_{0,avg}-p_{0,60^\circ avg}}{q}$$

$$PR = P_{0,\ AIP} \ / \ P_{0,in}$$

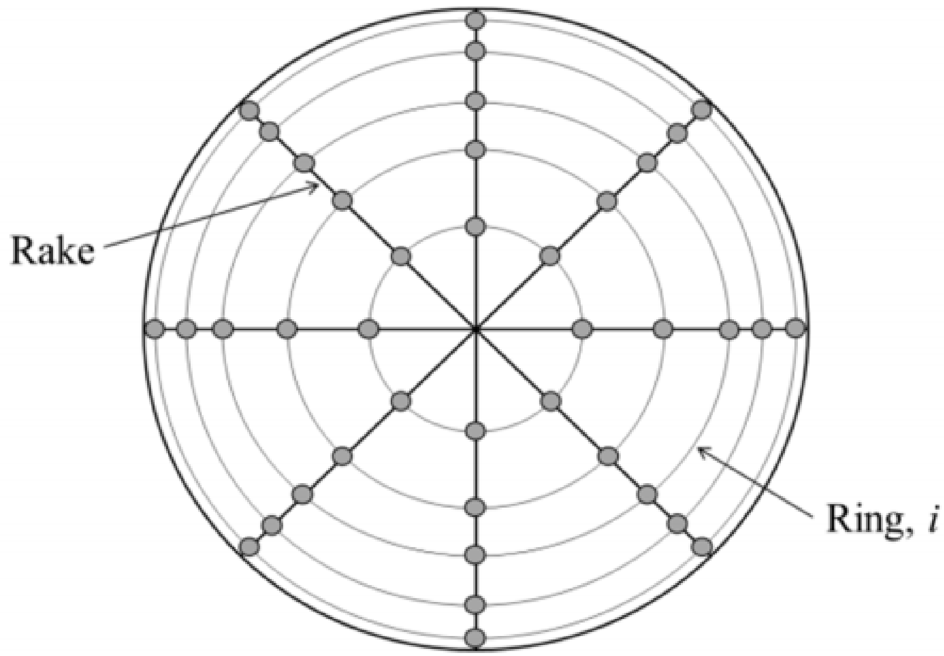

8 x 5 ring and rake AIP discretisation

Total pressure distortion descriptor reconstruction – Time averaged descriptor accuracy

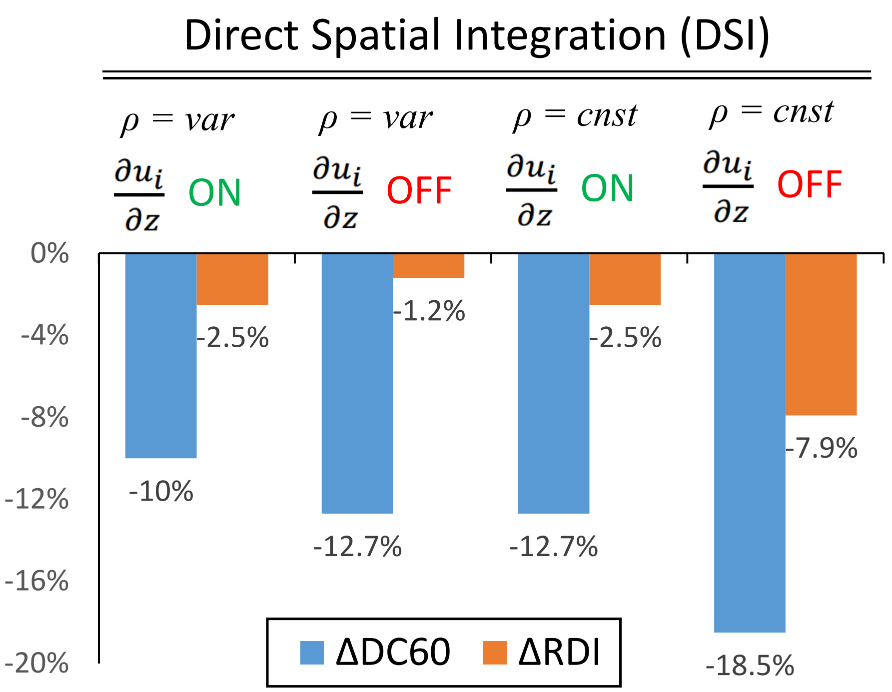

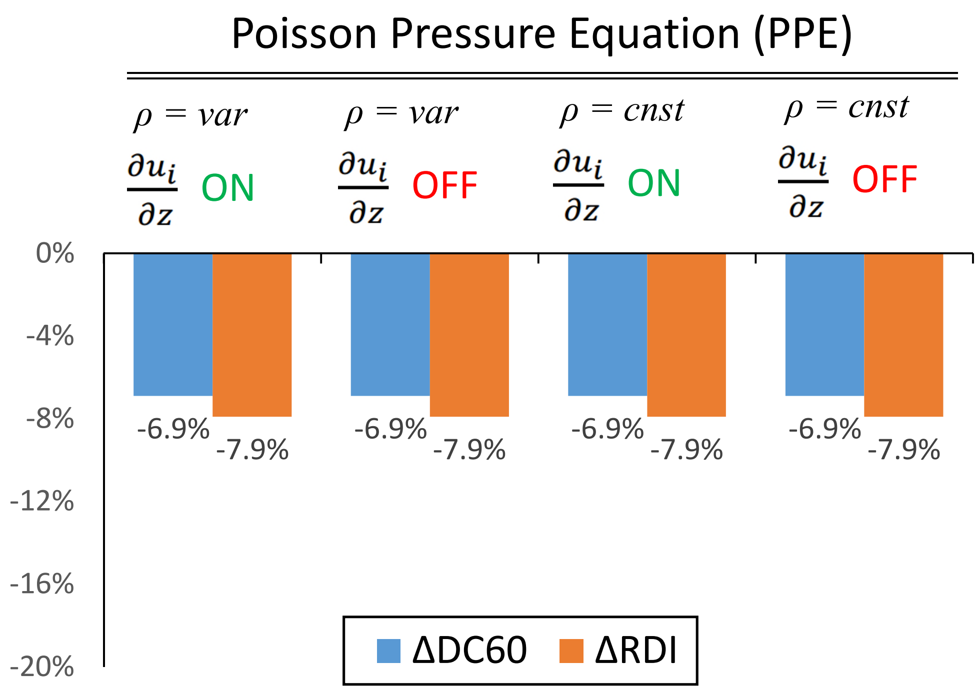

Discrepancy between reconstructed and CFD descriptor:

$$\Delta x = \frac{x_{rec} - x_{CFD}}{x_{rec}}$$

- ❑ DSI DC60 influenced by treatment of density and out-of-plane velocity terms
- ❑ Lower discrepancies in PR/RDI/CDI
- ❑ PPE consistently under-predicts all descriptors by appr. 8%
- ❑ PPE less susceptible to density and out-of-plane terms treatment

Total pressure distortion descriptor reconstruction with DSI – Unsteady descriptor accuracy

$\rho = var$ $\quad \frac{\partial u_i}{\partial z}$ ON $\quad \frac{\partial u_i}{\partial t}$ ON

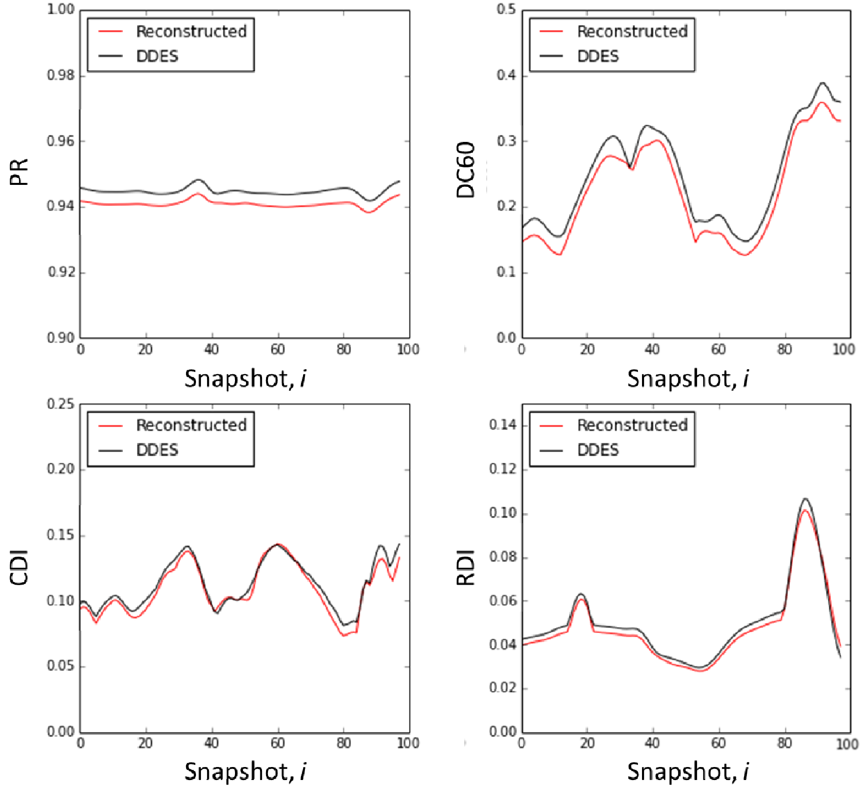

$\rho = var$ $\quad \frac{\partial u_i}{\partial z}$ OFF $\quad \frac{\partial u_i}{\partial t}$ OFF

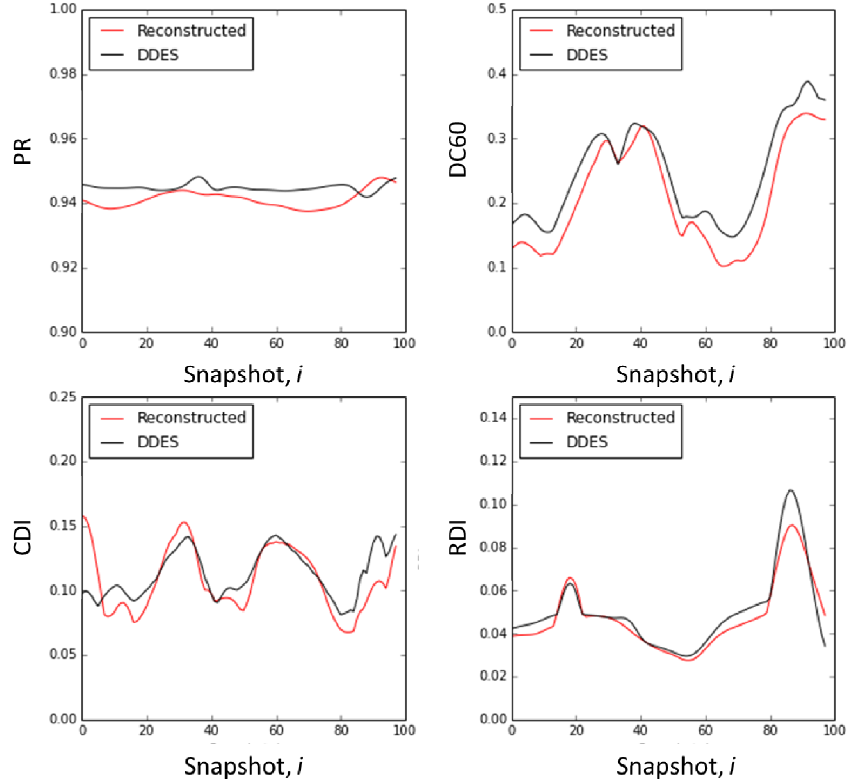

Total pressure distortion descriptor reconstruction with DSI – Unsteady descriptor accuracy

Cranfield UNIVERSITY

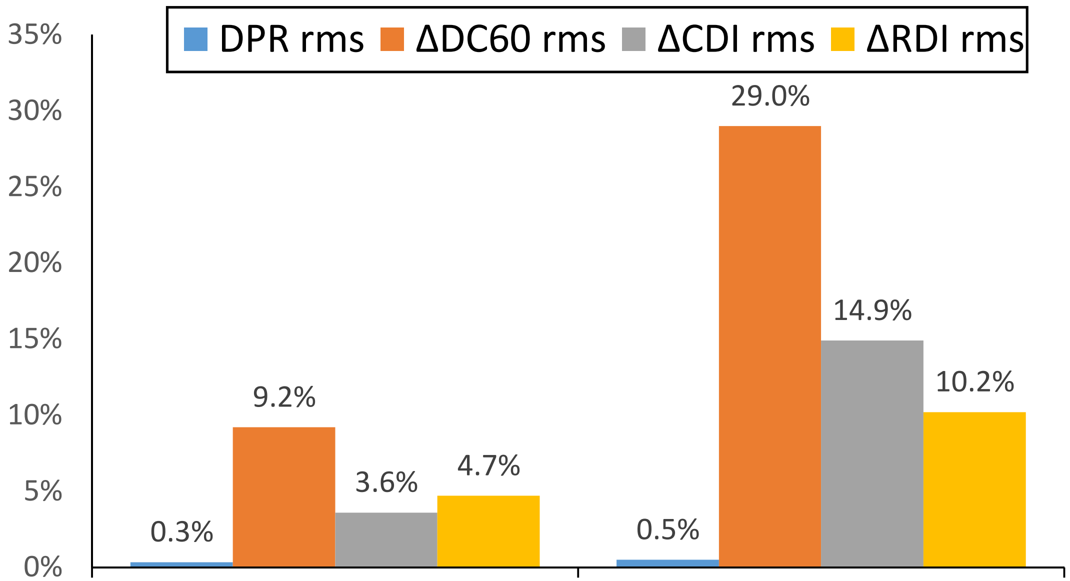

$\rho = var$ $\frac{\partial u_i}{\partial z}$ ON $\frac{\partial u_i}{\partial t}$ ON

$\rho = var$ $\frac{\partial u_i}{\partial z}$ OFF $\frac{\partial u_i}{\partial t}$ OFF

Discrepancy of reconstructed descriptor time series from DDES:

$$\Delta x_{rms} = \sqrt{\frac{\sum_{i=1}^{n}(\Delta x)^2}{n}}$$

- ❑ PR remains un-affected by the treatment of out-of-plane velocity terms
- ❑ RDI x2 higher uncertainty
- ❑ DC60/CDI x3 higher uncertainty

Impact of boundary condition – Steady BC / steady DSI reconstruction

Cranfield UNIVERSITY

Steady DSI reconstruction with $\rho = var$ and $\frac{\partial u_i}{\partial z}$ ON

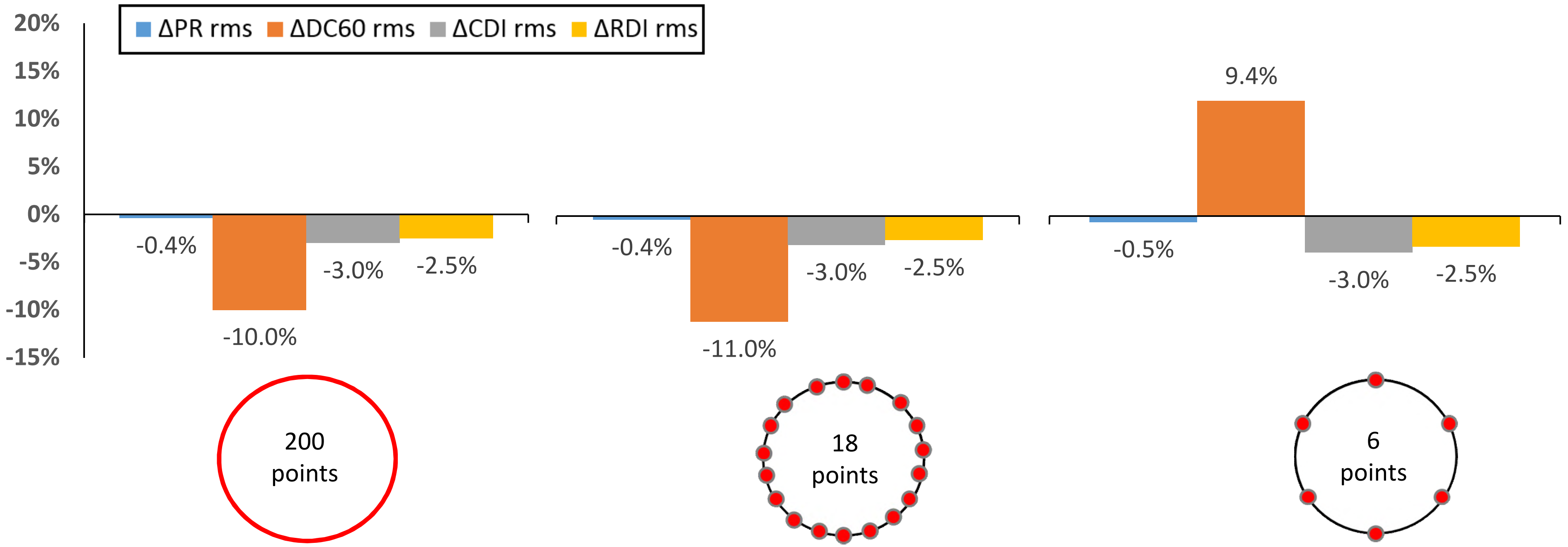

Discrepancy between reconstructed and CFD descriptor: $\Delta x = \frac{x_{rec} - x_{CFD}}{x_{rec}}$

Impact of boundary condition – Unsteady BC / unsteady DSI reconstruction

Unsteady DSI reconstruction with $\rho = var$, $\frac{\partial u_i}{\partial z}$ ON and $\frac{\partial u_i}{\partial t}$ ON

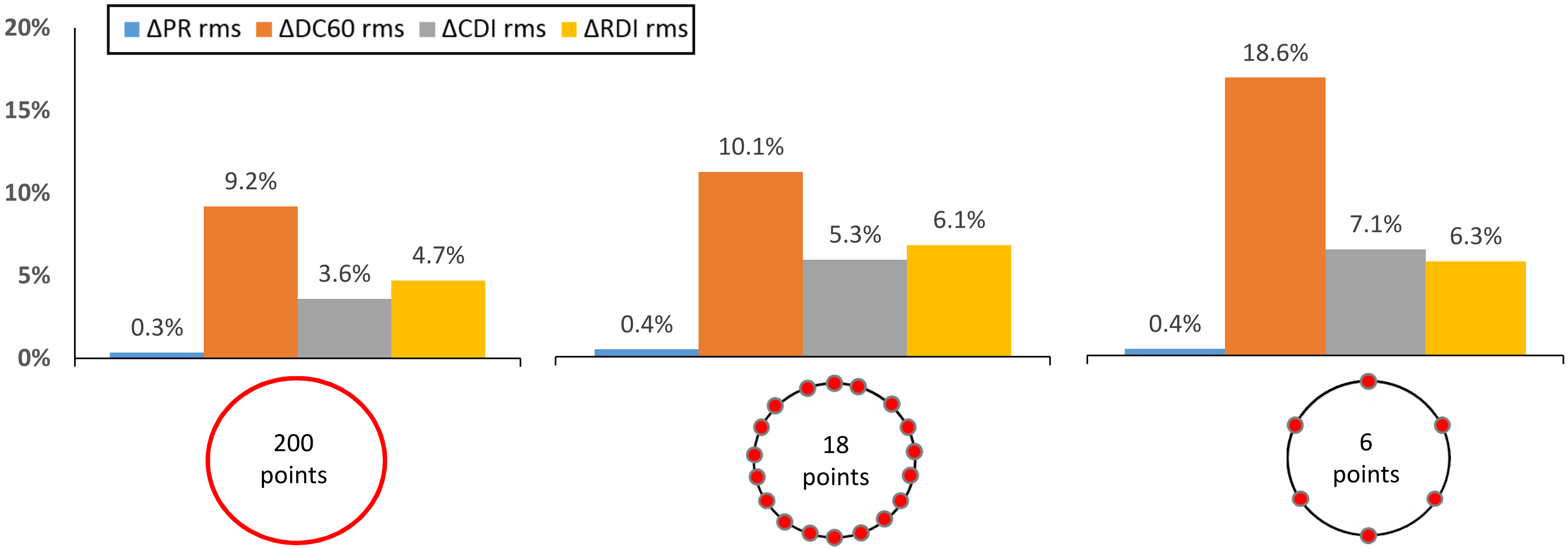

Discrepancy of reconstructed descriptor time series from DDES: $\Delta x_{rms} = \sqrt{\frac{\sum_{i=1}^{n}(\Delta x)^2}{n}}$

Impact of boundary condition – Steady BC / unsteady DSI reconstruction

Unsteady DSI reconstruction with $\rho = var$, $\frac{\partial u_i}{\partial z}$ ON and $\frac{\partial u_i}{\partial t}$ ON

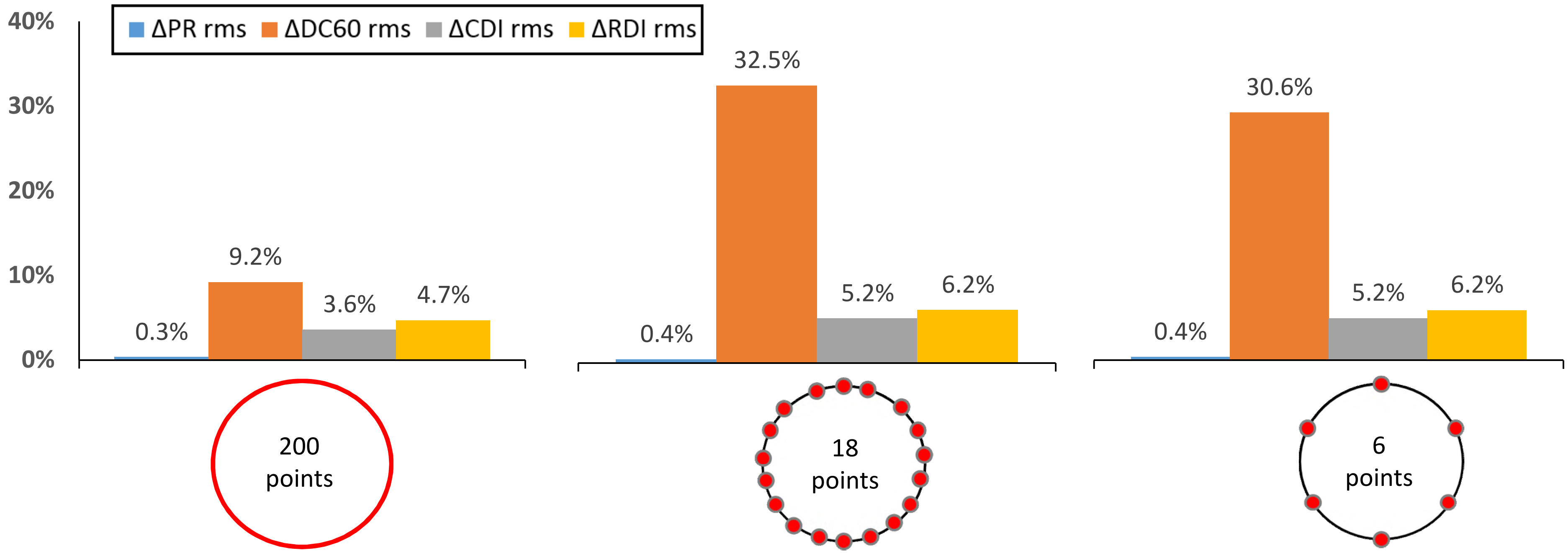

Discrepancy of reconstructed descriptor time series from DDES: $\Delta x_{rms} = \sqrt{\frac{\sum_{i=1}^{n}(\Delta x)^2}{n}}$

Wrap up

1. Pressure fields at the exit plane of complex intakes reconstructed from velocimetry data
2. Synchronous coupling of swirl and total pressure distortion metrics with high spatial resolution
3. Less intrusive instrumentation
4. Time-average reconstruction:
   - DSI – functional – susceptible to density and out-of-plane velocity gradient treatment
   - PPE – functional – better accuracy – less influenced by density and out-of-plane velocity gradient treatment
   - Max calculated uncertainty appr. -19% (DSI reconstructed DC60 from planar velocity data and constant density)
5. Unsteady reconstruction:
   - DSI – functional
   - <15% uncertainty for PR/CDI/RDI – appr. 30% uncertainty in DC60
   - PPE – more worked needed!
6. Impact of boundary conditions:
   - DC60 primarily affected by nature and resolution of static pressure distribution along the boundary
   - Low impact of number & nature of boundary points on PR/CDI/RDI reconstruction
   - Potential to reconstruct unsteady distortion metrics with a low resolution, steady BC

In conclusion…

- ✓ S-PIV provides a step change in measurement capability
- ✓ Velocimetry data can be further exploited in conjunction with Hi-Fi numerical methods
- ✓ …even to reconstruct flow properties (pressure fields)
- ✓ Advanced processing methods are very powerful if used wisely

Recent papers on the topic

1. Pavlos Zachos, David G. MacManus, and Nicola Chiereghin. "Flow distortion measurements in convoluted aero engine intakes", *33rd AIAA Applied Aerodynamics Conference*, AIAA 2015-3305, Dallas, TX, USA. – **In press AIAA Journal**

2. David G. MacManus, Nicola Chiereghin, Daniel Gil Prieto, and Pavlos Zachos. "Complex aero-engine intake ducts and dynamic distortion", *33rd AIAA Applied Aerodynamics Conference,* AIAA 2015-3304, Dallas, TX, USA. **Under review AIAA Journal**

3. Gil Prieto, D., **Zachos, P., K.,** MacManus, D., G., Tanguy, G., "Convoluted Intake distortion measurements using stereo PIV", *34th AIAA Applied Aerodynamics Conference,* AIAA 2016-3560, Washington DC, USA.

4. Gil Prieto, D., MacManus, D., G., **Zachos, P., K.,** Tanguy, G., Wilson, F., Chiereghin, N., "Dynamic Flow distortion investigation in S-ducts using DDES and SPIV data", *34th AIAA Applied Aerodynamics Conference,* AIAA 2016-3562, Washington DC, USA.

5. Frascella, M., **Zachos, P., K.,** Gil Prieto, D., MacManus, D., G., "Pressure flow field and inlet flow distortion metrics reconstruction from velocity data", *34th AIAA Applied Aerodynamics Conference,* AIAA 2016-3561, Washington DC, USA.

6. Tanguy, G., **Zachos., P., K.**, MacManus., D., Gil Prieto, D., "Passive flow control study in a convoluted intake using stereo particle image velocimetry", *34th AIAA Applied Aerodynamics Conference,* AIAA 2016-3563, Washington DC, USA.

Complex aero engine intake aerodynamics

Cranfield UNIVERSITY

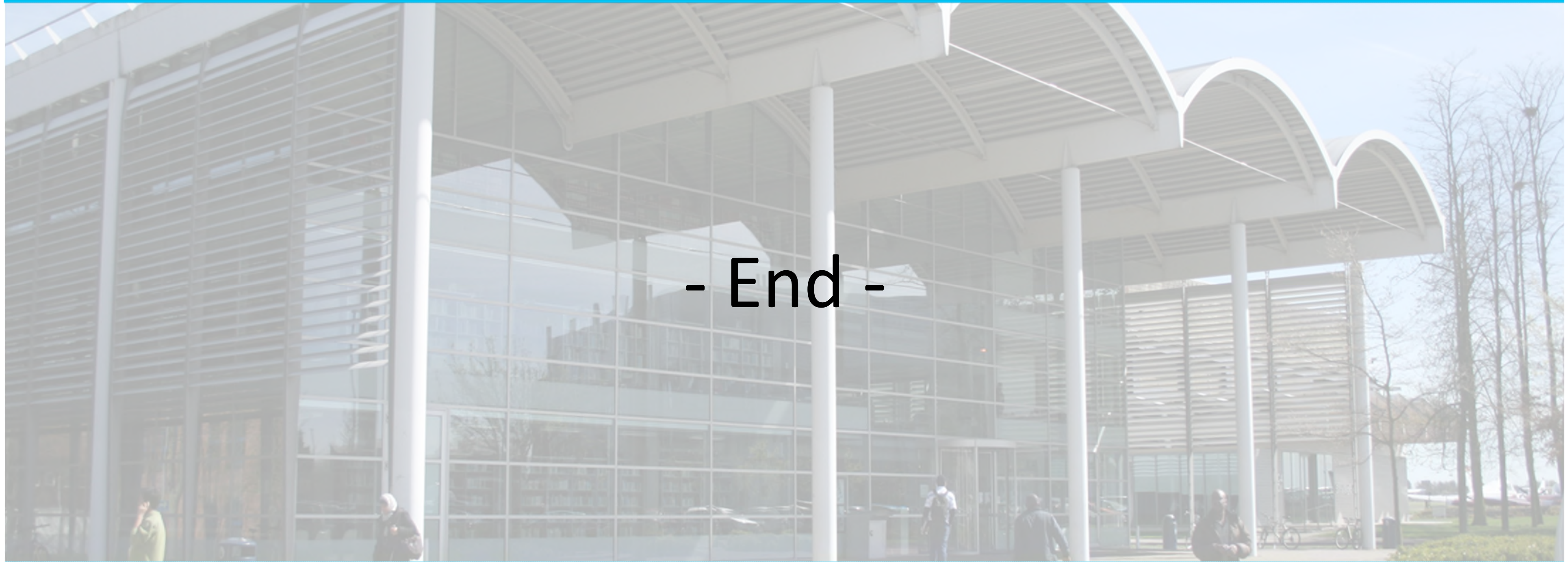

- End -

Pavlos K Zachos, David G. MacManus, Daniel Gil

Propulsion Engineering Centre - Cranfield University, United Kingdom

XXIII Biannual Symposium on Measuring Techniques in Turbomachinery, Transonic and Supersonic Flows in Cascades and Turbomachines, Stuttgart, Germany 2016